AD-A252 677

# INVESTIGATION OF A CESIUM RAMAN TIME/FREQUENCY STANDARD

Massachusetts Institute of Technology

Shaoul Ezekiel

DTIC
ELECTE
JUL 0 8 1992
S B

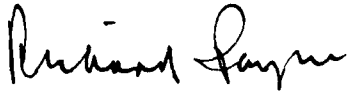*APPROVED FOR PUBLIC RELEASE; DISTRIBUTION UNLIMITED.*

92-17570

92 7 06 036

Rome Laboratory
Air Force Systems Command
Griffiss Air Force Base, NY 13441-5700

This report has been reviewed by the Rome Laboratory Public Affairs Office (PA) and is releasable to the National Technical Information Service (NTIS). At NTIS it will be releasable to the general public, including foreign nations.
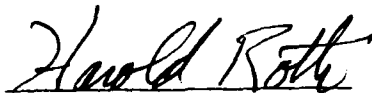
RL-TR-91-413 has been reviewed and is approved for publication.

APPROVED:

RICHARD PAYNE, Chief
Electro-Optical Device Tech Division

FOR THE COMMANDER:

HAROLD ROTH, Director
Solid State Sciences Directorate

# REPORT DOCUMENTATION PAGE

Form Approved
OMB No. 0704-0188

| 1. AGENCY USE ONLY (Leave Blank) | 2. REPORT DATE | 3. REPORT TYPE AND DATES COVERED |
|---|---|---|
| | December 1991 | Final     Mar 86 – Jun 89 |

**4. TITLE AND SUBTITLE**

INVESTIGATION OF A CESIUM RAMAN TIME/FREQUENCY STANDARD

**6. AUTHOR(S)**

Shaoul Ezekiel

**5. FUNDING NUMBERS**

C  -  F19628-86-K-0002
PE -  61102F
PR -  LDFP
TA -  05
WU -  C6

**7. PERFORMING ORGANIZATION NAME(S) AND ADDRESS(ES)**

Massachusetts Institute of Technology
Research Laboratory of Electronics
Cambridge MA 01239

**8. PERFORMING ORGANIZATION REPORT NUMBER**

N/A

**9. SPONSORING/MONITORING AGENCY NAME(S) AND ADDRESS(ES)**

Rome Laboratory (ERO)
Hanscom AFB MA 01731-5000

**10. SPONSORING/MONITORING AGENCY REPORT NUMBER**

RL-TR-91-413

**11. SUPPLEMENTARY NOTES**

Rome Laboratory Project Engineer:  Philip R. Hemmer/ERO/ (617) 377-5170
This effort was funded totally by the Laboratory Director's fund.

**12a. DISTRIBUTION/AVAILABILITY STATEMENT**

Approved for public release; distribution unlimited.

**12b. DISTRIBUTION CODE**

**13. ABSTRACT (Maximum 200 words)**

The objective of this program was to determine the feasibility of developing an improved portable cesium clock using a semiconductor laser excited resonance Raman interaction.  Such a clock has the potential to be smaller, lighter, less expensive, and more accurate than conventional cesium clocks because it does not require a microwave cavity or state selection magnets.  To demonstrate this, an experimental Raman cesium clock was constructed.  To excite the Raman transition in this beam, a semiconductor laser was amplitude modulated at 4.6 GHz (half of the 9.2 GHz cesium hyperfine transition frequency) so that the two modulation sidebands were tuned to the resonance Raman transition frequency.  The observed signal to noise ratio of about 1800 for a 2 second averaging time was detector noise limited, but only a factor of two smaller than the shot noise limit.  For a 15 cm interaction zone separation, such as in the experimental Raman clock, this signal to noise ratio cooresponds to a fractional frequency stability of $6 \times 10^{-12}$ (for a 100 second averaging time).  This compares favorably with commercial cesium clocks.  Once detector noise is eliminated, the shot noise limited fractional stability would be $2.7 \times 10^{-12}$ (for 100 sec.).

**14. SUBJECT TERMS**

Cesium Clocks,  Atomic Beams, Raman Scattering, Semiconductor Lasers

**15. NUMBER OF PAGES**

**16. PRICE CODE**

| 17. SECURITY CLASSIFICATION OF REPORT | 18. SECURITY CLASSIFICATION OF THIS PAGE | 19. SECURITY CLASSIFICATION OF ABSTRACT | 20. LIMITATION OF ABSTRACT |
|---|---|---|---|
| UNCLASSIFIED | UNCLASSIFIED | UNCLASSIFIED | UL |

# ABSTRACT

The objective of this program was to determine the feasibility of developing an improved portable cesium clock using a semiconductor laser excited resonance Raman interaction. Such a clock has the potential to be smaller, lighter, less expensive, and more accurate than conventional cesium clocks because it does not require a microwave cavity or state selection magnets. To demonstrate this, an experimental Raman cesium clock was constructed using a compact, inexpensive atomic beam design which incorporated optical quality windows, a recirculating oven, and graphite getters. To excite the Raman transition in this beam, a semiconductor laser was amplitude modulated at 4.6 GHz (half of the 9.2 GHz cesium hyperfine transition frequency) so that the two modulation sidebands were tuned to the resonance Raman transition frequency. A simple, alignment insensitive optical feedback stabilization scheme was developed for the semiconductor laser to obtain optimum signal to noise ratio, as well as to improve reliability of the laser. The observed signal to noise ratio of about 1800 for a 1 second averaging time was detector noise limited, but only a factor of two smaller than the shot noise limit. For a 15 cm interaction zone separation, such as in the experimental Raman clock, this signal to noise ratio corresponds to a fractional frequency stability of $6 \times 10^{-12}$ (for a 100 second averaging time). This compares favorably with commercial cesium clocks. Once detector noise is eliminated, the shot noise limited fractional stability would be $2.7 \times 10^{-12}$ (for 100 sec.). The instabilities caused by potential error sources are projected (from sodium studies) to be of the order of $2 \times 10^{-12}$.

## 1.  SUMMARY OF OBJECTIVES

The primary goal of this research program is to determine the possibility of developing a small, low cost, light weight, portable clock based on a laser-induced
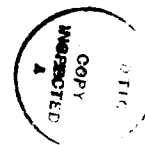
resonance Raman transition in a cesium atomic beam. Such a clock would employ semiconductor lasers to excite the atomic beam, rather than the conventional microwave cavities and state selection magnets. To demonstrate this, an experimental version of the cesium Raman clock is to be constructed, using only semiconductor laser excitation and a compact atomic beam design. Its accuracy is to be compared to that of a commercial cesium clock.

## 2. BRIEF REVIEW OF RESONANT RAMAN INTERACTION AND CLOCK APPLICATIONS

The laser induced resonance Raman interaction is illustrated schematically in Fig. 1(a). Briefly, Raman transitions are induced between states |1> and |3> using two laser fields, at frequencies $\omega_1$ and $\omega_2$, simultaneously resonant with the intermediate state |2>. The result of this simultaneous resonance is a decrease in the observed fluorescence, as shown in Fig. 1(b). For copropagating laser fields interacting with an atomic beam at right angles, the linewidth of this Raman transition is determined only by the widths of states |1> and |3>. State |2> does not contribute to the linewidth, although it clearly enhances the transition probability. Thus, for long-lived states |1> and |3>, the Raman linewidth becomes transit time limited just as for direct microwave excitation.

In practice, to observe transit time limited Raman lineshape, it is necessary to overcome the effects of laser jitter. This can be done by correlating the frequency jitters of $\omega_1$ and $\omega_2$. Correlated jitter does not broaden the Raman transition because it does not affect the laser difference frequency, $\omega_1 - \omega_2$. One way of correlating the frequency jitters is to generate both frequencies from the same laser; for example, the beam at frequency $\omega_2$ can be generated from the beam at frequency $\omega_2$ using an acousto-optic frequency shifter.

2

To obtain a small transit time linewidth we use Ramsey's method of separated field excitation in analogy with conventional microwave techniques. In separated field excitation, atom-field superposition states set up by the Raman interactions in the two zones interfere quantum mechanically. This produces interference fringes in the final zone fluorescence, where the fringe spacings are characteristic of the transit time between interaction zones.

To provide a stable reference for clock applications, the rf signal which drives the difference frequency generator (e.g., the acousto-optic modulator) is locked to the central Ramsey interference minimum. To accomplish this, a discriminant is needed and is generated by frequency modulating the rf signal and demodulating the final zone fluorescence signal with a lock-in amplifier. The output of the lock-in amplifier then provides the error signal for the rf frequency servo. The stability of the rf frequency is measured by comparing it with a commercial cesium (or rubidium) clock.

## 3. BRIEF DESCRIPTION OF RESULTS

The primary goal of this program was met by construction of an experimental Raman cesium clock, employing a compact yet inexpensive atomic beam design and a semiconductor laser, with a projected frequency stability that compares favorably with commercial cesium clocks. In order to help optimize the preliminary design of the cesium Raman clock, an existing experimental sodium Raman clock was used to investigate the effects of several frequency error sources such as the AC Stark shift, for example, that are present in both sodium and cesium Raman clocks.

### 3.1 Construction of an experimental Raman cesium clock

The experimental Raman cesium clock consisted of a compact atomic beam and a semiconductor laser. The laser was amplitude modulated and the two modulation sidebands were used as the two Raman excitation frequencies,

3

$\omega_1$ and $\omega_2$. Semiconductor laser optical feedback was employed to obtain optimum signal to noise, and also to improve reliability of the laser.

### 3.1.1 Atomic beam design

As stated before, the primary goal of the atomic beam design was to develop a beam that would be inexpensive and easily miniaturized. To these ends, we have designed a compact and low cost atomic beam, as shown schematically in Fig. 2.

The interaction region consists of a section of steel waveguide with knife edge vacuum flanges welded to both ends. Windows are placed at various locations in the waveguide, as shown, to admit laser light and to facilitate fluorescence detection. The windows are of good optical quality, and are anti-reflection coated. To mount the windows an o-ring sandwich is used, so as not to generate an unacceptable amount of stress related birefringence.

To maintain a low background pressure, each interaction port is supplied with a graphite getter, having holes bored along all three axes. The size of the hole along the atomic beam axis determines its collimation.

The atomic beam source consists of a porous metal rod inserted in a stainless tube, which in turn is welded to a knife-edge vacuum flange. The porous metal rod is bored with a 2 mm dia. hole and serves as a recirculating heat pipe oven[1]. In operation, the front section of the porous metal is kept just above the melting point of cesium, while the rear section is heated to a high temperature. Material not travelling along the axis of the porous metal sticks to the cold section and is returned to the

hot end by capillary action. This recirculating oven design permits a high throughput with a low source consumption.

### 3.1.2 Generation of second laser frequency

Generation of the two optical fields, at frequencies $\omega_1$ and $\omega_2$, was accomplished by modulating the semiconductor laser injection current at 4.6 GHz with a microwave VCO, as illustrated in Fig. 3. This yields two amplitude modulation sidebands that are separated by 9.2 GHz, the cesium hyperfine transition frequency. As discussed before, the frequency jitters of $\omega_1$ and $\omega_2$ are now correlated since the frequencies are generated from the same laser, thus eliminating the effects of laser jitter on the Raman linewidth. The carrier is detuned too far (4.6 GHz, or about a thousand linewidths of the cesium excited state) from either transition to have any effect at all. The laser diode used here is single frequency, double heterostructure, AlGaAs laser (Hitachi HLP-1400) operating at 852 nm.

Figure 4(a) shows the modulation sidebands of the modulated laser as measured by a short, plane-parallel, scanning Fabry-Perot cavity with a free spectral range of 25 GHz. As can be seen, the separation between sidebands is 4.6 GHz. In contrast, Fig. 4(b) shows the spectrum of the unmodulated single mode laser.

### 3.1.3 Initial observation of Raman/Ramsey fringes in a cesium beam using a wideband semiconductor laser

Using the above-mentioned unmodified semiconductor laser with a free running linewidth of 20 MHz, we have been able to observe a 1

kHz (limited by transit time) wide Raman-Ramsey fringe in the cesium beam. The schematic of the experimental setup is illustrated in Fig.3.

The output from the modulated laser interacts with the cesium atomic beam in zones A and B, and the fluorescence from zone B is collected onto a photodetector. Consider first the fluorescence when zone A is blocked. Figure 5(a) shows schematically the fluorescence expected as the laser frequency plus sidebands are scanned over the 1-2 and the 3-2 transitions. Three resonances are expected for each transition just as in the Fabry-Perot cavity scans of Fig. 4. However, when the modulation frequency is near 4.6 GHz, the fluorescence due to the upper sideband excitation of the 3-2 transition overlaps with that due to the lower sideband excitation of the 1-2 transition. Figure 5(b) shows the observed fluorescence resulting from these two overlapped transitions. The observed linewidth is about 35 MHz, which is primarily due to laser jitter since the natural linewidth of the cesium transition is 5 MHz and the residual Doppler broadening in the atomic beam is 2 MHz.

To observe a Raman transition, the laser frequency is held by a servo, near the maximum of the fluorescence lineshape in Fig. 5(b), and the microwave VCO frequency is scanned over a wide, 60 MHz range. As illustrated in Fig. 3, the servo is constructed by modulating the laser frequency at $f_1$ = 60 kHz, and demodulating the fluorescence signal with a phase sensitive demodulator to generate the discriminant.

Figure 6(a) shows the derivative of a single zone Raman transition as a function of microwave frequency, with zone A blocked and the laser circularly polarized. As can be seen, the observed linewidth is about 450 kHz, which is consistent with power broadening for our set up. The single zone transit time linewidth would be only 60 kHz. The derivative of

6

the Raman transition is shown because of its good signal to noise ratio. This derivative was generated by modulating the frequency of the microwave oscillator at $f_2$ = 550 Hz, and demodulating the fluorescence signal with another phase sensitive detector.

The Raman line in Fig. 6(a) is one of seven Zeeman transitions, shown in Fig. 6(b), that were observed with a 6 Gauss magnetic field applied parallel to the laser beam. It was necessary to lift the degeneracy of the magnetic sublevels to avoid the effects of local magnetic fields fluctuations. As shown in the figure, the separation between Zeeman lines is about 4 MHz, as expected for a 6 Gauss field.

To achieve a linewidth narrower than the single zone linewidth of 450 kHz, Ramsey's method[2] of separated fields excitation was employed by allowing the laser to interact with the atomic beams at zones A and B, (Fig. 3) separated by 15 cm. In this case, the demodulated fluorescence from zone B (Fig. 7) shows the Ramsey fringes as the microwave oscillator is slowly swept through the center of the m = 0, $\Delta$m = 0 Raman transition. The laser is circularly polarized with 1 mW of total power in both zones A and B, and a 4 to 1 carrier to sideband ratio. As shown in the figure, the central fringe has a width of just under 1 kHz, which is in good agreement with that predicted for a 15 cm interaction zone separation and a 200°C oven temperature. In addition, the shape of the Ramsey fringes in Fig. 7 is consistent with that expected for an atomic beam with a thermal velocity distribution. The fringe amplitude is nearly equal to the amplitude of the single zone Raman lineshape, as expected for a stable laser difference frequency and a collisionless atomic beam.

7

The observed signal to noise ratio for the Raman-Ramsey fringes was about 400 (for an averaging time of one second). This was about 10 times worse than the signal to noise ratio expected from the shot noise limit for the setup. The primary causes of the lower signal to noise were the large fluorescent background due to lack of magnetic shielding, and the fluorescence intensity fluctuations caused by the large laser frequency jitter.

To improve the signal to noise ratio, the interaction region was enclosed in a magnetic shielding, and efforts were undertaken to reduce the frequency jitter of the semiconductor laser using optical feedback techniques, as described below.

### 3.1.4. Optical feedback stabilization and tuning of the semiconductor laser

As seen above, the semiconductor laser had to be stabilized to generate a narrow linewidth. In addition, the laser had to be tunable continuously so that the desired cesium resonance could be excited. To achieve such goals, others have devised optical-feedback schemes that employ frequency selective elements, such as gratings or etalons in the feedback path[3]. However, all these optical-feedback techniques require the use of antireflection-coated lasers and, in addition, are highly sensitive to alignment of the external optics. These factors detract from the simplicity and low cost inherent in semiconductor lasers.

To circumvent these new problems, we have devised our own frequency-selective self-aligning optical feedback technique that allows a semiconductor laser to be tuned to and scanned about any optical frequency within the laser gain curve. This technique uses a graded-

8

index rod (GRINROD) lens cat's eye reflector (i.e. retroreflector) and an intracavity etalon. Most importantly we use unmodified commercial semiconductor lasers with no special anti-reflection coatings.

The basic laser optical feedback setup is shown in Fig. 8. The output of an off-the-shelf semiconductor laser is first collimated by a 0.22 pitch antireflection-coated plano-convex GRINROD lens and then filtered by the tilted solid etalon (optical thickness 0.15 mm, 80% reflectivity). Next, this light is reflected back into the laser by the uncoated rear surface of a 0.25-pitch GRINROD lens mounted on a piezoelectric transducer (PZT) cylinder. This GRINROD lens serves as a one-piece cat's eye reflector. Because of the self-aligning nature of the cat's eye reflector, the external cavity consistently maintains its alignment so that there is no need to provide any adjustments for fine angular alignment. Typical feedback light levels used in this experiment are of the order of 0.25%, and the total cavity length is about 10 cm. For a 1-mm optical path length semiconductor laser cavity having 30% facet reflectivity, this results in a theoretical linewidth reduction factor of 55[4].

The passband of the etalon is tuned by adjusting its tilt angle mechanically. By adjusting the etalon passband, the semiconductor laser can be forced to lase in a longitudinal mode that is different from the main mode. Once the longitudinal mode has been selected, the laser can be tuned continuously, within the external cavity free spectral range, by changing the length of the external cavity with the PZT. For longer range continuous-frequency scans, it is necessary to vary the injection current in synchronization with the external cavity length, which can be done either open-loop or with a servo.

9

We have demonstrated the applicability of this optical feedback technique to the excitation of a cesium resonance by employing a nominally 852-nm Ortel SL 300 laser. Figure 9 shows a series of traces obtained by ramping the laser current, i, from the threshold to the highest current while monitoring the laser intensity after it passes through a cesium vapor cell. Figure 9(a) shows data obtained without optical feedback for a variety of different laser temperatures. As can be seen, the laser excites cesium efficiently only for one combination of temperature and current, i.e., the top trace. With our optical feedback setup, however, it is possible to excite cesium at a variety of temperatures, as shown in Fig. 9(b). These cesium absorptions were obtained by simply tilting the etalon at each temperature until a strong cesium absorption was found. These data illustrate that reliable tuning to an atomic resonance such as cesium is possible even though the laser may not excite the resonance without optical feedback.

Figure 10 shows a typical scan of the cesium $D_2$ hyperfine components in a cesium vapor cell using a semiconductor laser with optical feedback as described above. Here, laser absorption is monitored as a function of laser frequency. The continuous scan range here is about 20 GHz. The measured linewidth of the laser was less than 3 MHz, which is consistent with the prediction of factor-of-55 reduction, given the 125 MHz free running linewidth of the laser used.

### 3.1.5 Improvement of observed signal to noise ratio

With the semiconductor laser stabilized via optical feedback, we have repeated the experiment reported in section 3.1.3. The laser used is Ortel SL 300, with a linewidth of less than 3 MHz, which is much

10

narrower than the width (20 MHz) of the laser used in the experiment of section 3.1.3. In addition, we have used a magnetic shield around the atomic beam.

With these improvements, we have been able to observe, in cesium, a Raman-Ramsey fringe pattern of a much higher signal to noise ratio. Figure 11 shows a typical pattern of Raman-Ramsey fringes observed this way. The observed signal to noise ratio of about 1800 for a 1 second averaging time was detector noise limited, but only a factor of two smaller than the shot noise limit. For a 15 cm interaction zone separation, such as in our experiment, this signal to noise ratio corresponds to a fractional frequency stability of $6 \times 10^{-12}$ (for a 100 second averaging time).

## 3.2 Error source studies

Once the detector noise limitation is eliminated, the stability of our experimental cesium Raman clock is expected to be shot noise limited up to a certain averaging time. The magnitude of this averaging time is the measure of the long term stability of the clock. This magnitude is limited by various error sources that cause the clock frequency to drift in the long term. Identification and control of these error sources are necessary to improve the performance of the cesium Raman clock.

In this regard, the knowledge gained from our studies done with an experimental sodium Raman clock can be used as a starting point. With this in mind, we continued analyses of experimental results obtained from the sodium Raman clock error source studies. In particular, the effect of AC Stark shift was studied extensively with encouraging results. In addition, we have analyzed the various error sources that are common to both sodium and cesium Raman

11

clocks so as to project the magnitude of the effects in the cesium clock from those in the sodium clock.

Clearly it would be better to perform error source studies directly on the Raman Cesium clock. However, the optical feedback techniques have not yet been sufficiently refined to permit the laser to be locked to cesium for an extended period of time (hours to days) which would be needed for an error source study.

### 3.2.1 AC Stark effect in sodium Raman clock

The AC Stark effect is a major cause of concern in any optically excited atomic clock. For the Raman clock AC Stark shifts are expected to occur if both laser frequencies, $\omega_1$ and $\omega_2$, are detuned from resonance by the same amount (termed common mode detuning). Such a detuning can be caused by laser frequency drift or laser misalignments.

We have measured the AC-Stark effect in a two zone stimulated Raman interaction in a sodium atomic beam. In addition, we have derived simple theoretical expressions for the AC-Stark shift, based on a closed three level system, in the $\Lambda$ configuration, and have achieved qualitative agreement with the data. In particular, the magnitude and sense of the AC-Stark shifts are found to depend on laser intensities as well as on the initial populations of the two low lying levels of the $\Lambda$ configuration. Specifically, the AC-Stark shifts are smaller for large laser intensities, and also for smaller initial population differences between the two low lying levels. Moreover, the AC-Stark shift is shown to be insensitive to the ratio of the intensities of the two lasers, provided the sum of the two intensities is fixed. The AC-Stark shift is also shown to be insensitive to changes in laser beam profiles as long as the time

12

integrated intensity as seen by the moving atom remains unchanged. Quantitative agreement between ideal three level theory and experiment is improved when the effects of the numerous Zeeman sublevels in sodium are taken into account to first order. Finally, the experimentally observed reversal of AC-Stark shift was used in identifying conditions under which the AC-Stark shift can be reduced to levels low enough to be acceptable for potential clock applications.

The data of Fig. 12(a) demonstrates an AC-Stark shift of less than 0.0014 radian over a laser detuning of nearly $\pm 0.2y_2$. Figure 12(b) is the AC-Stark shift predicted by our theoretical calculations, showing good agreement. For clock applications, this corresponds to a projected stability of better than $2 \times 10^{-11}$ (for sodium) for a laser detuning of $0.01y_2$ (100 kHz). Here is should be noted that this result is still preliminary and does not represent the ultimate achievable clock performance. Nonetheless, this data demonstrates that by proper choice of experimental conditions, the AC-Stark shift can be greatly reduced, even within the limitations of the present experimental setup.

### 3.2.2  Projected effects of various error sources in cesium

Based on the knowledge gained from the error source studies in a sodium Raman clock, we can project the effects of some of the error sources in the cesium Raman clock. As will be seen, many of the more important error sources for sodium are much less critical for cesium. Only path length related phase shifts are expected to be more important for cesium. These projections are summarized in Table 1.

13

### 3.2.2.1 Relative misalignment

If the two laser beams at frequencies $\omega_1$ and $\omega_2$ intersect the atomic beam at different angles, the differences in the optical Doppler shifts cause a shift in the clock frequency. For separated field excitation, the clock shift is much smaller than the optical Doppler shift. In sodium, the observed fractional error is about $5 \times 10^{-7}/0.1$ mrad. In cesium, the fractional error would be smaller by a factor of about 70. This includes a factor of 1.4 lower for optical frequency, 5.1 for higher hyperfine splitting, and about 9.3 for atomic velocity, where the velocity factor includes both the effects of a smaller Doppler shift and smaller fringe width.

In sodium, this error was minimized by making the two laser fields exactly copropagating by passing them through a common single mode fiber. The fiber used in our experiment however, was single mode only to 1 part in $10^5$, resulting in a fractional error of about $5 \times 10^{-12}/0.1$ mrad, where 0.1 mrad is a typical value of misalignment at the fiber input. In cesium, this would correspond to a fractional error of about $7 \times 10^{-14}/0.1$ mrad. However, in cesium the two frequencies are expected to be copropagating to much better than 0.1 mrad because of the way they are generated via amplitude modulation.

### 3.2.2.2 Optical phase shift

The relative phases of the electrical fields at frequencies $\omega_1$ and $\omega_2$ in zones A and B (Fig. 3) determines the "phase" of the Ramsey fringes. For example, a differential path length change of half an optical wavelength, which effects only the $\omega_1$ component in

14

zone A would result in a shift in the clock frequency by a full Ramsey fringe linewidth. Optical path length shifts of this magnitude can arise if there are birefringent optics present and if $\omega_1$ and $\omega_2$ do not have identical polarization. This effect should be smaller for cesium by a factor of about 16. This includes a factor of 5.1 for higher hyperfine splitting, and 3.1 for slower velocity.

In sodium, this error is minimized by using a linear polarizer immediately after the optical fiber. For a polarizer good to 1 part in $10^6$, the residual fractional error due to 0.1 wavelength birefringence in the optics is about $1 \times 10^{-13}$. For the cesium clock, however, direct amplitude modulation should generate sidebands of identical polarization.

### 3.2.2.3  Path length phase

In the absence of birefringence, the relative phase of the electric fields at frequencies $\omega_1$ and $\omega_2$ varies with path length changes on the order of a microwave wavelength (17 cm for sodium). For example, a change in the relative pathlengths from the beamsplitter of Fig. 3 to zones A and B by half a microwave wavelength, would result in the clock frequency shift equal to the Ramsey fringe linewidth. In cesium, the resulting fractional error would only be smaller by a factor of 3 because of the slower velocity. The larger transition frequency also contributes a factor of 5, but this is cancelled by a factor of 5 due to the smaller cesium microwave wavelength.

In sodium, this effect is minimized by using an equal pathlength interferometer configuration[4] wherein the beam in

15

zone A is reflected back along zone B and vice versa, forming standing waves. For a 100 to 1 ratio of the standing wave to the residual traveling wave, the fractional error is about $2 \times 10^{-12}$ for a 0.01 mm path length difference; which is an easy distance accuracy to achieve when the clock is in operation. In cesium, this would project to a fractional error of about $7 \times 10^{-13}$.

### 3.2.2.4 Laser detuning and intensity

If the two laser frequencies, $\omega_1$ and $\omega_2$, are detuned from resonance by the same amount (common mode detuning), the clock frequency is shifted due to the AC-Stark effect, as discussed in section 3.2.1. The amplitude of this shift depends also on the laser intensity, and on the initial difference in populations between the two ground state levels. The AC-Stark shift, in absolute frequency, is proportional to the Ramsey fringe width. Thus the fractional clock error for a given Ramsey fringe phase shift would be a factor of 16 smaller in cesium because of differences in transit time and transition frequency.

#### 3.2.2.4.1 Common mode laser detuning

Common mode detuning can result from laser frequency fluctuations and drifts. In the cesium clock, errors due to common mode laser detuning would be smaller by a factor of about 8 than for sodium. This includes a factor of 16 for transition frequency and transit time but is reduced by a factor of 2 for the smaller intermediate state linewidth in cesium.

16

Common mode detuning can also result from laser misalignments, where the two frequencies are misaligned by the same angle, thus seeing equal Doppler shifts. In that case, the error in cesium would be smaller by a factor of about 25. This includes the factor of 8 from above plus additional factor of 3.1 for Doppler shift.

As discussed in detail in section 3.2.1, the AC-Stark shift can potentially be totally eliminated. For now, however, the effect can be highly minimized by choosing the proper operating conditions, as illustrated in Fig. 12. A typical magnitude, as reported therein, of the fractional error is about $2 \times 10^{-11}/100$ kHz. In cesium, this corresponds to a fractional error of about $2.5 \times 10^{-12}/100$ kHz using the factor of 8 from above.

### 3.2.2.4.2  Laser intensity

Changes in laser intensity can affect the clock frequency due to the AC-Stark shift, as discussed above. In addition, intensity changes can affect the clock frequency due to other mechanisms, such as the background slope effect. In cesium, intensity changes would produce smaller errors; a factor of 25, as discussed above, for the AC-Stark effect, and a factor of 16 for the background slope effect.

In sodium, the background slope effect has been reduced by about a factor of 100 using the third harmonic[4], instead of the first harmonic, demodulation to generate the discriminant (where a factor of 2 in signal to noise is lost).

17

Using the third harmonic technique, the residual Stark shift error in sodium is about $2 \times 10^{-12}$ for a 1% change in laser intensity. In cesium this projects to an error of about $1.3 \times 10^{-13}$ for a 1% change in laser intensity.

## 4.   Summary and Recommendations

An experimental cesium Raman clock has been constructed, employing a compact and inexpensive atomic beam, and a semiconductor laser stabilized by optical feedback. The observed signal to noise ratio of about 1800 was detector noise limited, but only a factor of 2 smaller than the value expected from shot noise. For a 15 cm interaction zone separation, such as in the experimental Raman clock, this signal to noise ratio corresponds to a fractional frequency stability of $6 \times 10^{-12}$ (for a 100 seconds averaging time). This compares favorably with commercial cesium clocks. Once detector noise is eliminated, the shot noise limited fractional stability would be $2.7 \times 10^{-12}$ (for a 100 seconds averaging time). The instabilities caused by potential error sources are projected (from sodium studies) to be of the order of $2 \times 10^{-12}$, as summarized in Table 1. Further investigations are needed to verify the projections made here.

## 5. References

1.  R.E. Drullinger etal, "A recirculating oven for atomic beam frequency standards", 39th Annual Symposium on Frequency Control IEEE Catalog No. 85CH2186-5 (1985).

2.  N.F. Ramsey, Molecular Beams, (Oxford Univ. Press, London, 1963).

3.  References 1 through 11 in B.E. Bernacki etal, "Alignment insensitive technique for wideband tuning of an unmodified semiconductor laser", Optics Letters, Vol. 13, No. 9, September 1988.

4.  L. Goldberg etal, IEEE JQE, QE-18, 555 (1982).

## 6. Publications

Enclosed are the publications relating to the progress reported here.

1.  P.R. Hemmer, H. Lamela-Rivera, S.P. Smith, B.E. Bernacki, M.S. Shahriar and S. Ezekiel, "Observation of Ultra-Narrow Ramsey Raman Fringes in a Cesium Atomic Beam Using a Semiconductor Laser", submitted to Optics Letters.

2.  B.E. Bernacki, P.R. Hemmer, S.P. Smith and S. Ezekiel, "Alignment-insensitive technique for wideband tuning of an unmodified semi-conductor laser", Optics Letters, Vol. 13, No. 9, September 1988.

3.  P.R. Hemmer, V.D. Natoli, M.S. Shahriar, B. Bernacki, H. Lamela-Rivera, S.P. Smith and S. Ezekiel, "Study of several error sources in a laser Raman clock", 41st Annual Frequency Control Symposium, 1987.

4.  P.R. Hemmer, M.S. Shahriar and S. Ezekiel, "AC Stark shift in a two zone Raman interaction", JOSA B, Vol. 6, No. 8, August 1989.

## Table 1

### Projected Effects of Error Sources in a Cesium Raman Clock

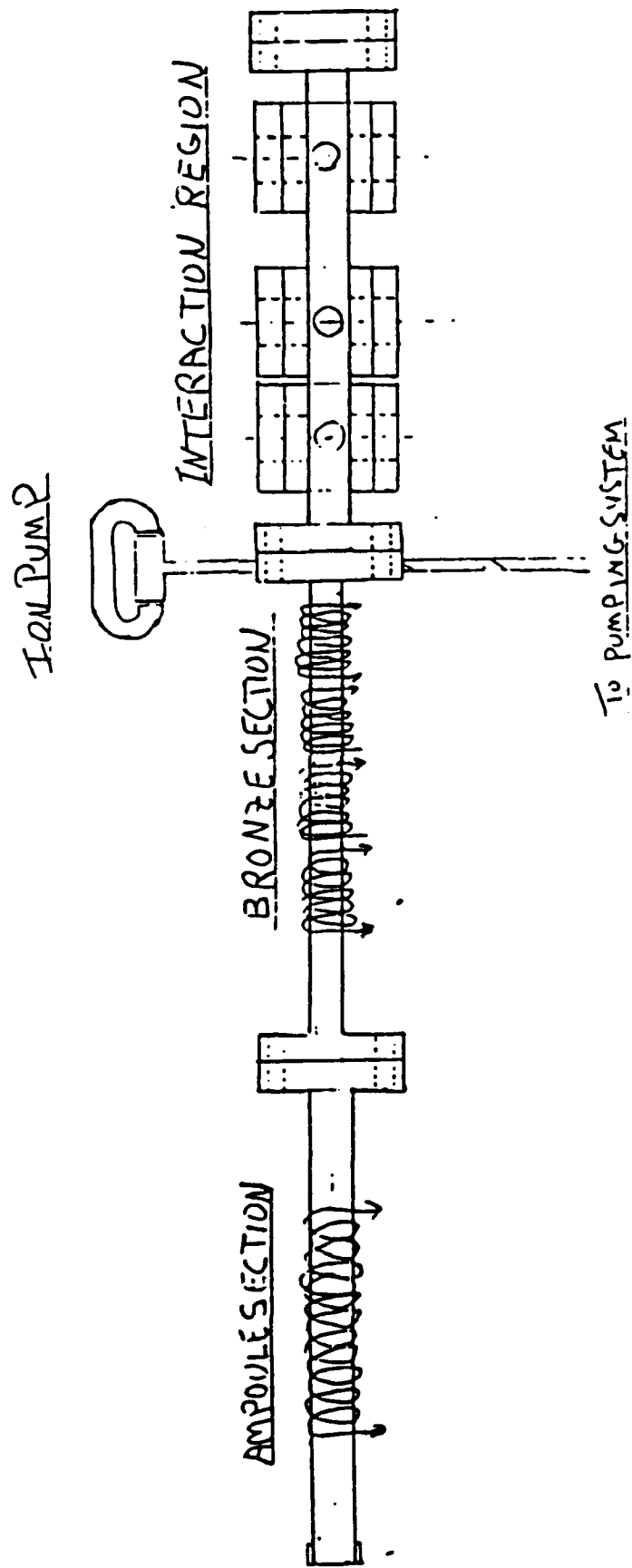| Error Source | Typical Fractional Error in Sodium | Sodium to Cesium Reduction Factor | Typical Fractional Error in Cesium |
|---|---|---|---|
| Relative Misalignment | $5 \times 10^{-12}$ / 0.1 mrad | 70 | No misalignment of modulation sidebands |
| Optical Phase Shift | $1 \times 10^{-13}$ / 0.1 $\lambda$ | 16 | Same polarization for both sidebands |
| Path Length Phase | $2 \times 10^{-12}$ / 0.01 mm | 3 | $7 \times 10^{-13}$ / 0.01 mm |
| Common Mode Detuning | $2 \times 10^{-11}$ / 100 kHz | 8 | $2.5 \times 10^{-12}$ / 100 kHz |
| Laser Intensity Change | $2 \times 10^{-12}$ / 1% change | 16 | $1.3 \times 10^{-13}$ / 1% change |
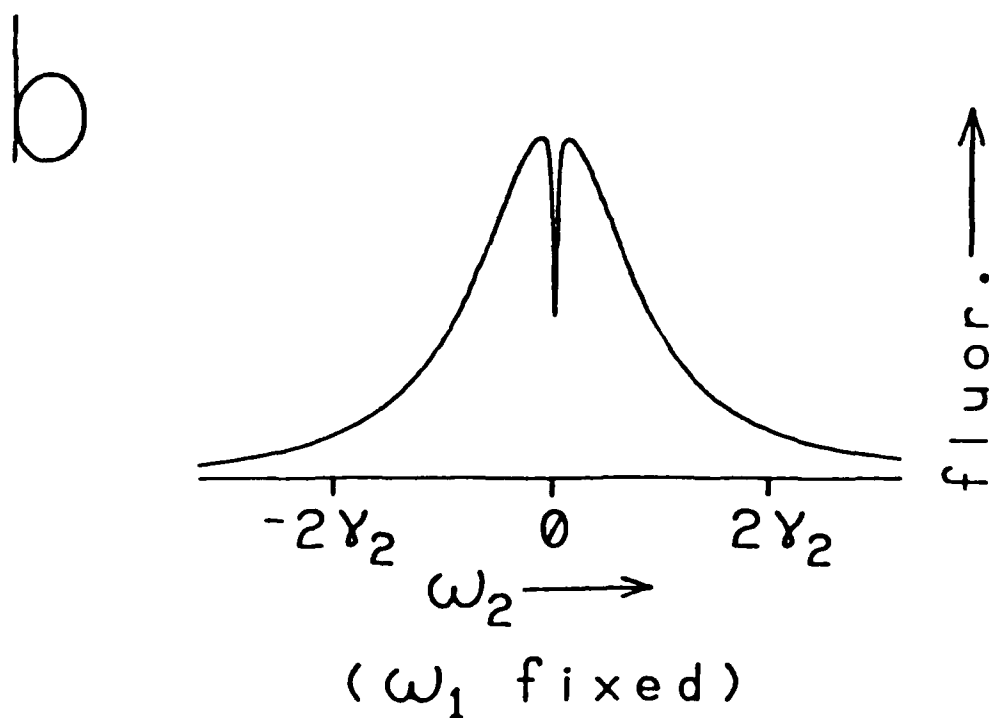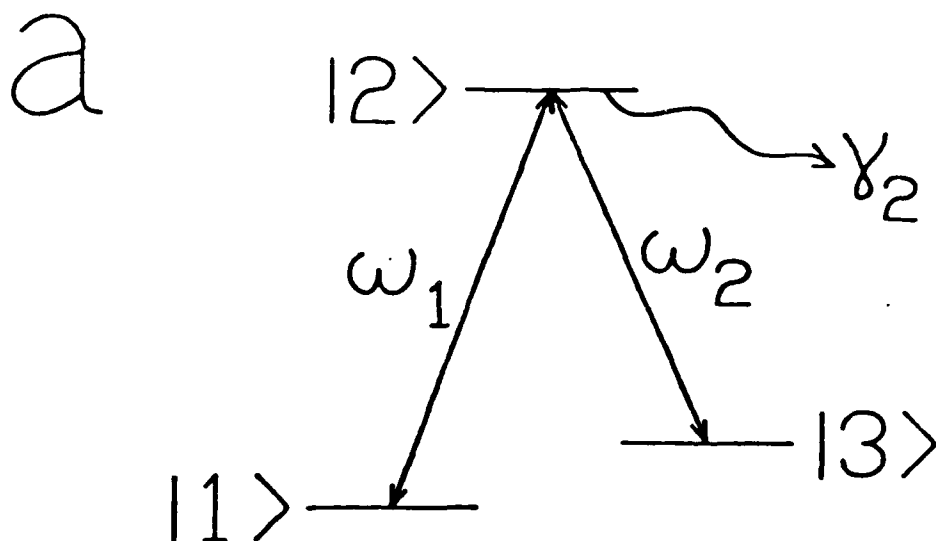
Fig. 1. Schematic of the resonant Raman scattering.
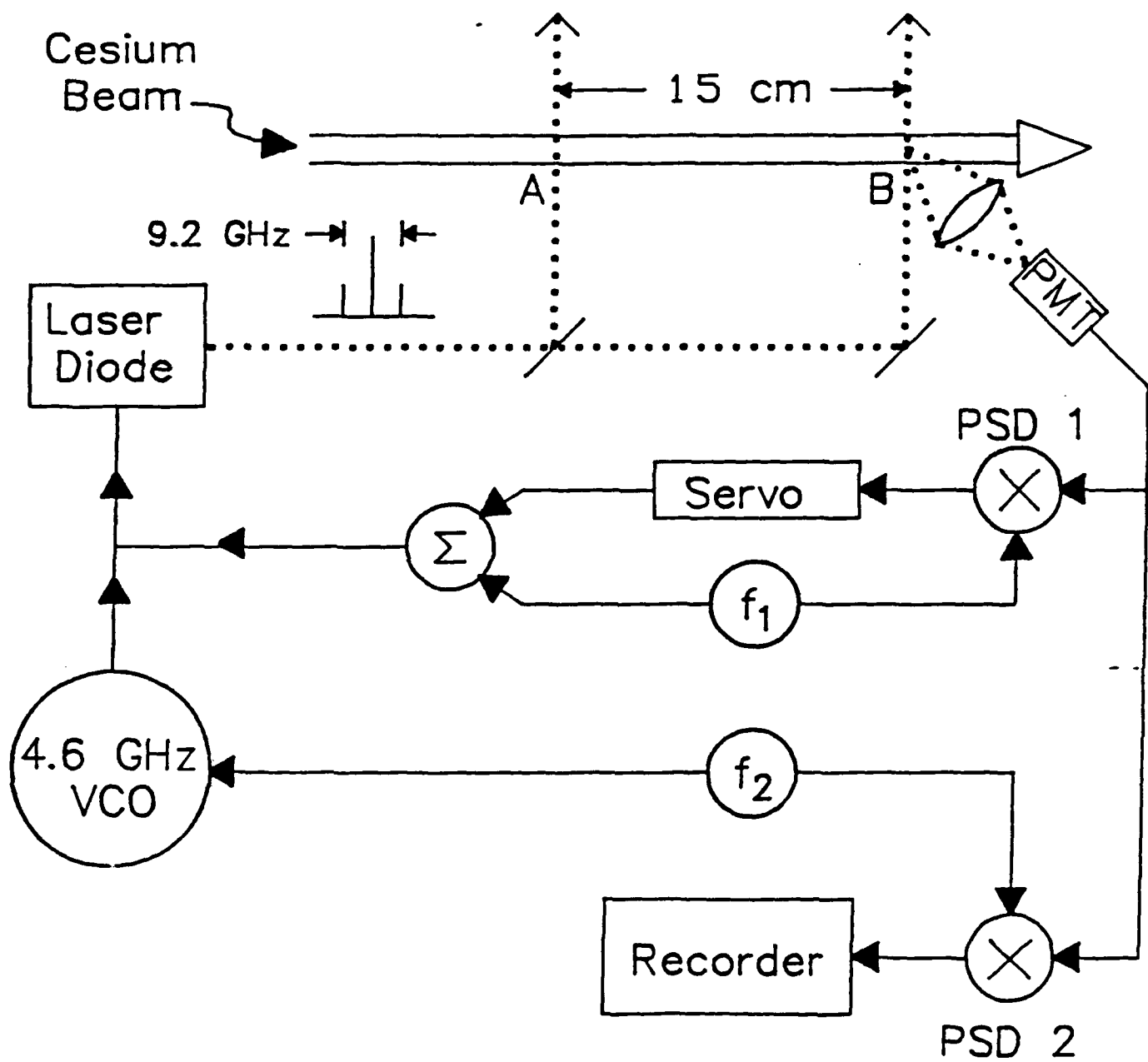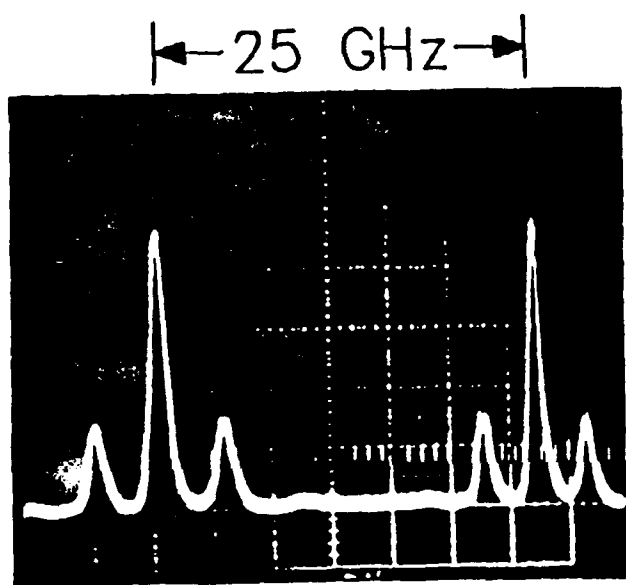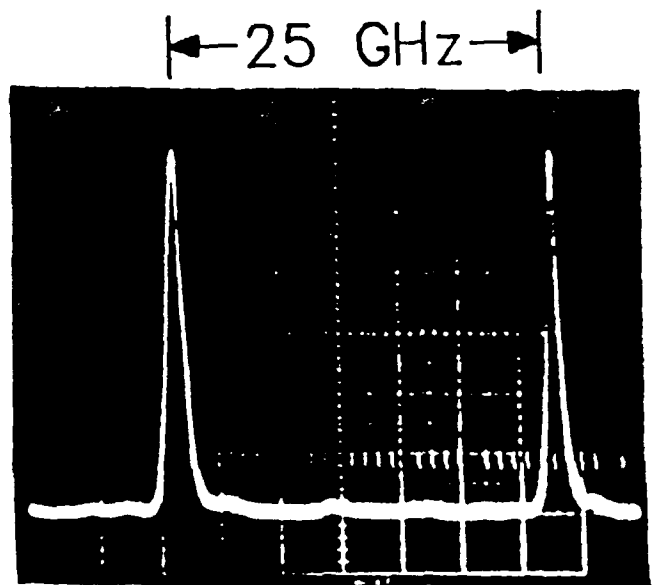
FIG.2. Schematic of the atomic beam apparatus

AMPOULE SECTION

BRONZE SECTION

ION PUMP

INTERACTION REGION

TO PUMPING SYSTEM

23

Fig. 3. Experimental set up

24

Fig. 4        Spectrum of : (a)  Modulated laser at 4.6 GHz
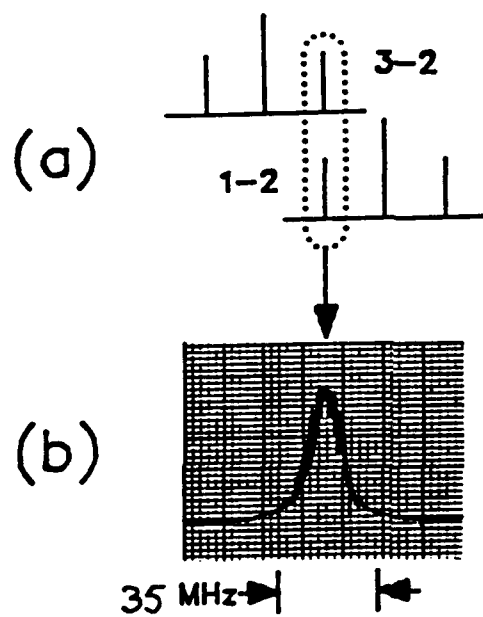
(b) Unmodulated laser

Fig. 5    Single zone cesium fluorescence when laser sidebands are

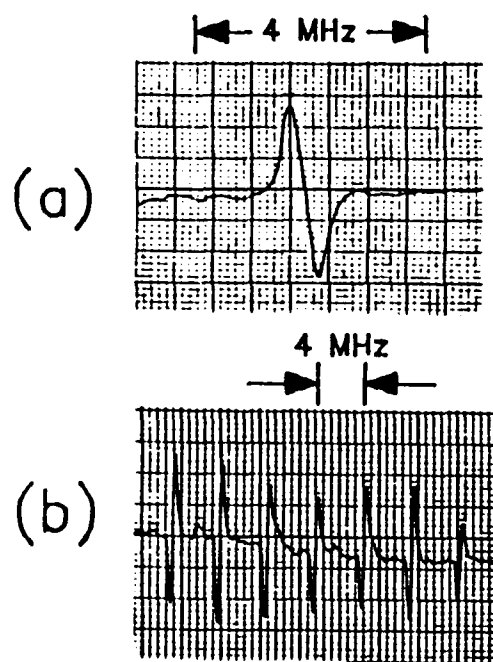scanned over 1-2 and also 3-2 transition

Fig. 6    (a) Expanded single zone Zeeman Raman transition in cesium

(b) Single zone Zeeman components of Raman transition in cesium
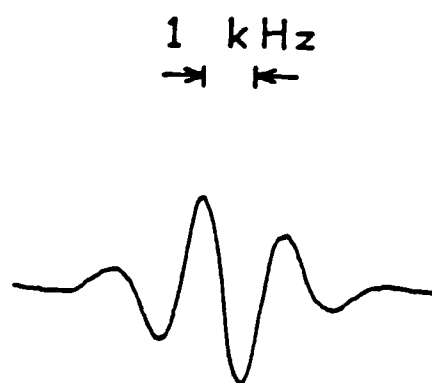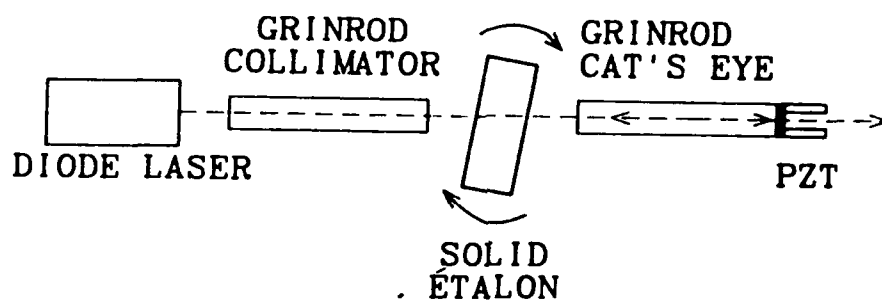
Fig. 7. Raman-Ramsey Fringes.

Fig. 8. Schematic of the alignment insensitive optical feedback.
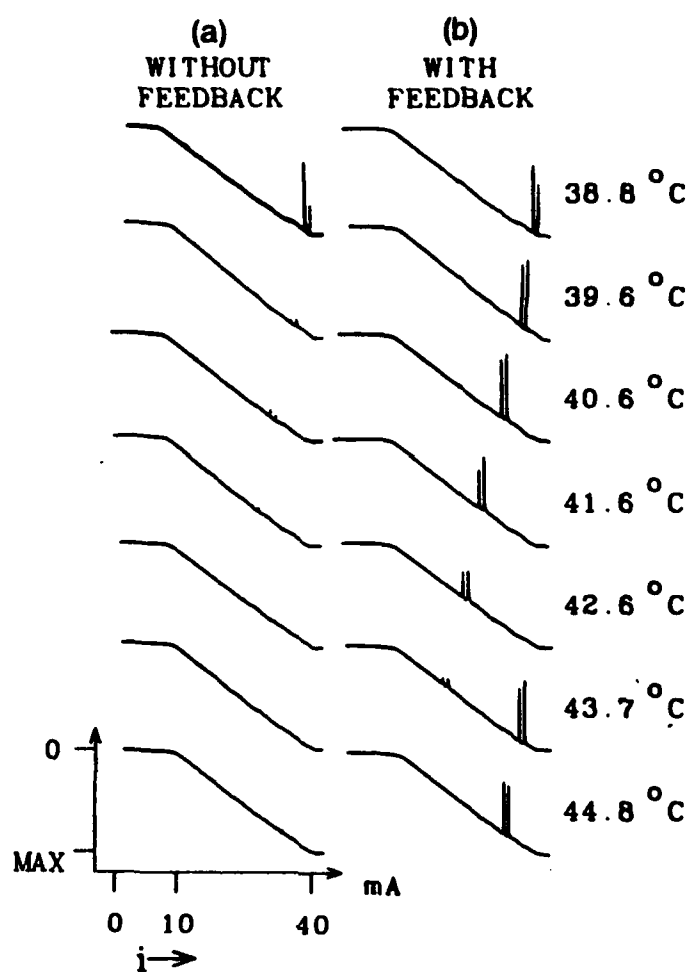
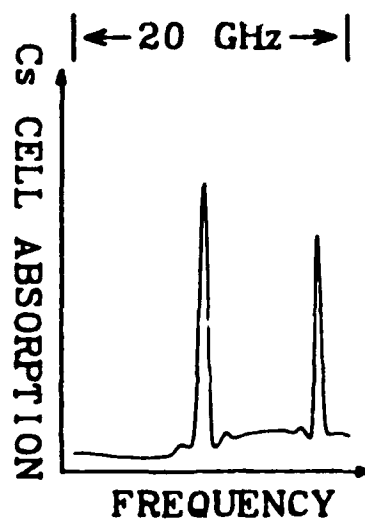Fig. 9.    Absorption of cesium vapor cell versus laser current.

Fig. 10. Continuous laser frequency scan over cesium $D_2$ hyperfine components in a vapor cell. Total scan range is 20 GHz.
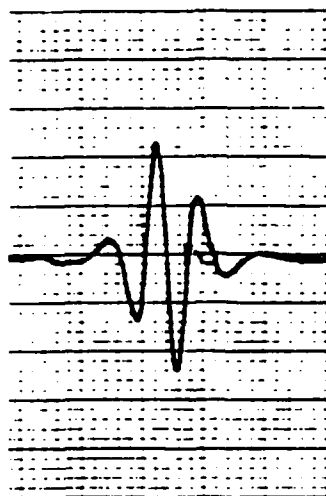
Fig. 11. Raman-Ramsey fringes obtained with a stabilized laser
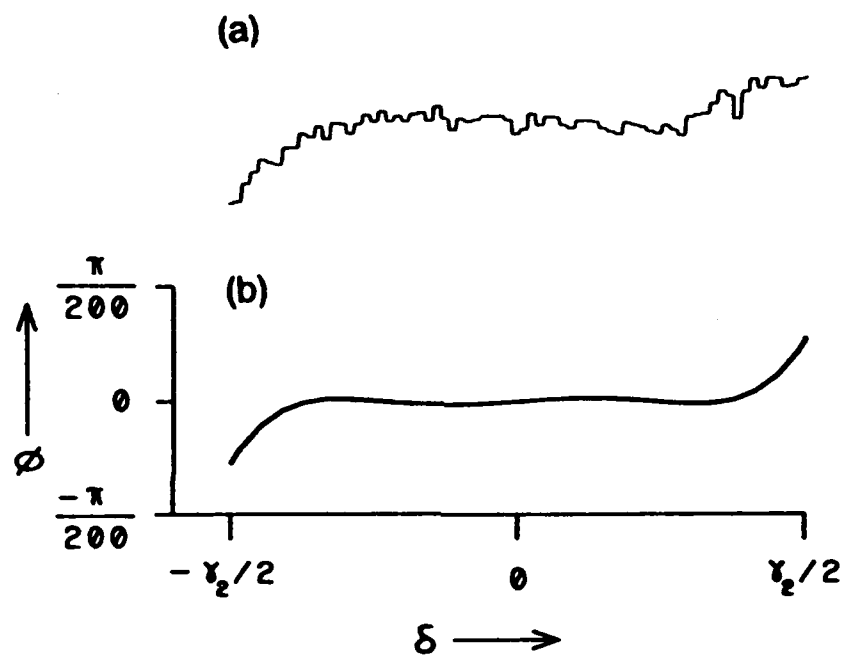
Fig. 12. High resolution scan of AC-Stark shift
as a function of common mode laser
detuning (a) Experimental (b) Theoretical

# OBSERVATION OF ULTRA-NARROW RAMSEY RAMAN FRINGES IN A CESIUM ATOMIC BEAM USING A SEMICONDUCTOR LASER

P.R. Hemmer*, H. Lamela-Rivera, S.P. Smith, B.E. Bernacki*

M.S. Shahriar and S. Ezekiel

Research Laboratory of Electronics

Massachusetts Institute of Technology

Cambridge, MA 02139

## ABSTRACT

A modulated semiconductor laser with a free running linewidth of 20 MHz has been used to excite a 9.2 GHz Raman transition in a cesium beam. Using Ramsey's separated field excitation, a 1 kHz wide Ramsey Raman fringe was observed. Application to the development of a compact, low cost time reference is discussed.

* Permanent Address: Rome Air Development Center (RADC/ESO)

Hanscom Air Force Base, MA 01731-5000

In this letter, we report the observation of an ultra narrow, 1 kHz wide Ramsey Raman fringe in a cesium atomic beam using a semiconductor laser with a large free running linewidth of 20 MHz. The significance of this experiment lies in the development of a long term stable time reference based on the Raman effect that could be an alternative to the cesium clock. A cesium Raman clock excited by a semiconductor laser could be smaller, lighter, and less expensive than the current cesium clock.

The stimulated resonance Raman process is illustrated in figure 1 where we show a Raman transition between two long-lived states, 1 and 3, induced by two laser fields at frequencies $\omega_1$ and $\omega_2$. As is well known[1,2], the Raman transition linewidth for weak copropagating laser fields is primarily determined by the decay rates of the long lived states 1 and 3. Thus, the linewidth is set by the transit time. To achieve an effectively long transit time, and thus a very narrow linewidth, Ramsey's technique of separated field excitation is used[3].

In our present experiment, the long-lived states 1 and 3 in figure 1 are respectively the 6 $^2S_{1/2}$ (F=3) and (F=4) ground state hyperfine levels in cesium separated by 9.2 GHz, and state 2 is the 6 $^2P_{3/2}$ (F=4) level. The optical transitions are components of the cesium $D_2$ line at 852 nm.

The experimental setup is shown schematically in figure 2. The laser diode is a single frequency, double heterostructure, AlGaAs laser (Hitachi HLP-1400) operating at 852 nm and mounted on a thermoelectric device. Figure 3 shows

the laser spectrum as measured by a confocal, scanning Fabry-Perot cavity with a 3 MHz instrumental linewidth and a free spectral range of 300 MHz. As shown in the figure, the laser linewidth is about 20 MHz.

Generation of the two optical fields, $\omega_1$ and $\omega_2$ is accomplished by modulating the laser current at 4.6 GHz with a microwave VCO, shown in figure 2, thus yielding two amplitude modulation sidebands separated by 9.2 GHz. By generating $\omega_1$ and $\omega_2$ in this manner, the effect of laser jitter can be eliminated.

Figure 4(a) shows the modulation sidebands of the modulated laser as measured by a short, plane-parallel, scanning Fabry-Perot cavity with a free spectral range of 25 GHz. As can be seen, the separation between sidebands is 4.6 GHz. In contrast, figure 4(b) shows the spectrum of the unmodulated single mode laser.

As indicated in figure 2, the output from the modulated laser interacts with the cesium atomic beam in zones "A" and "B", and the fluorescence from zone "B" is collected with a photomultiplier tube. First, we consider the fluorescence when zone "A" is blocked. Figure 5(a) shows schematically the fluorescence as the modulated laser frequency (carrier and sidebands) is scanned over the 1—2 and also the 3—2 transitions, shown in figure 1. As can be seen, three resonances are expected for each transition. However, when the modulation frequency is near 4.6 GHz, the fluorescence due to the excitation of the 3—2 transition by the upper sideband overlaps with the fluorescence due to the excitation of the 1—2

transition by the lower sideband. Figure 5(b) shows the observed fluorescence resulting from these two overlapped transitions. The linewidth in this case is about 35 MHz, which is primarily due to laser jitter since the natural linewidth of the cesium transition is 5 MHz and the residual Doppler broadening in the atomic beam is 2 MHz .

To observe a Raman transition, the laser is held by means of a servo, near the maximum of the fluorescence lineshape in Fig. 5(b), and the microwave VCO frequency is scanned over 60 MHz. As illustrated in figure 2, the servo consists of modulating the laser current at $f_1 = 60$ kHz, and demodulating the fluorescence signal in a phase sensitive demodulator (PSD 1) to generate the discriminant needed for the servo.

Figure 6(a) shows the derivative of a single zone resonance Raman transition as a function of microwave frequency, with zone "A" blocked and the laser circularly polarized. As can be seen in the figure, the observed linewidth is 450 kHz which is consistent with power broadening for our set up since the single zone transit time linewidth is about 60 kHz. We have used the derivative of the Raman transition to enhance the signal to noise ratio. This derivative was generated by modulating the frequency of the microwave oscillator at $f_2 = 550$ Hz, and demodulating the fluorescence signal with PSD 2.

The Raman line in figure 6(a) is one of seven Zeeman transitions, shown in figure 6(b), observed when a 6 Gauss magnetic field was applied parallel to the

laser beam. It was necessary to lift the degeneracy of the magnetic sublevels to avoid the effects of local magnetic fields. As shown in the figure, the separation between Zeeman lines is about 4 MHz, as expected for a 6 Gauss field.

To achieve a linewidth narrower than the single zone linewidth of 450 kHz, we employed Ramsey's method[3] of separated fields excitation by allowing the laser to interact with the atomic beam at zones "A" and "B", separated by 15 cm. In this case, the demodulated fluorescence from zone "B" (Fig. 7) shows the Ramsey fringes as the microwave oscillator is slowly swept through the center of

the m=0, $\Delta$m=0, Raman transition. The laser is circularly polarized with

1 mW of total power in both zones A and B and a 4 to 1 carrier to sideband ratio. As shown in the figure, the central fringe has a width of just under 1 kHz, which is in good agreement with that predicted for a 15 cm interaction zone separation

and a 200°C oven temperature. In addition, the shape of the Ramsey fringes in Figure 7 is consistent with that expected for an atomic beam with a thermal velocity distribution. The fringe amplitude is nearly equal to the amplitude of the single zone Raman lineshape, as expected for a stable laser difference frequency and a collisionless atomic beam.

The presently observed signal to noise ratio is 400 for a 1 sec time constant. This is about 10 times worse than the shot noise limit expected for the present set up. The primary causes of the lower signal to noise are the large fluorescence background at present and the fluorescence intensity fluctuations caused by the large laser frequency jitter. Semiconductor lasers, with less frequency jitters, on

the order of 1 MHz, are available and could be used to reduce such intensity fluctuations. To minimize the fluorescence background we will need to employ magnetic shielding of the interaction region. Thus, if we assume shot-noise-limited detection, the fractional frequency stability would be $3 \times 10^{-11}/\tau^{1/2}$ and this would compare well with commercially available cesium clocks. The signal-to-noise can, of course, be improved further by increasing the atomic beam throughput as is presently being pursued in optically pumped cesium clocks.[4]

Future work will be focussed on the study of error sources in semiconductor laser excited cesium Raman clocks. Preliminary experiments performed on the sodium Raman clock excited with a dye laser showed that all major sources of long term drift, including the light shifts, can be controlled experimentally.

Since semiconductor lasers are also available at 780 nm near the resonance excitation of rubidium, it would be worthwhile to consider a rubidium Raman clock in addition to cesium. Also, we wish to consider simple methods of laser cooling the cesium beam[6] to increase the transit time for a given zone separation and oven temperature. Finally the possibility of a millimeter wave Raman clock[3] is also being explored.

39

## References

1.  M.S. Feld, M.M. Burns, T. V. Kuhl, P.G. Pappas, & D.E. Murnick, Opt. Lett. 5, 79 (1980).

2.  R.P. Hackel & S. Ezekiel, Phys. Rev. Lett. 42, 1736 (1976) & references therein.

3.  J.E. Thomas, P.R. Hemmer, S. Ezekiel, C.C. Leiby,Jr., R. H. Picard & C.R. Willis, Phys. Rev. Lett. 48, 867 (1982).

4.  M. Arditi & J.L. Picque, J de Phys. 41, L-379 (1980); "Optically Pumped Small Cesium Beam Standards: A Status Report", A. Derbyshire, R.E. Drullinger, M. Feldman, D.J. Glaze, D. Hilliard, D.A. Howell, L.L. Louis, J.H. Shirley, I. Pascaru, D. Stanciulescu, 39th Annual Symposium on Frequency Control, Philadelphia, May 1985, p. 18.

5.  P.R. Hemmer, V.D. Natoli, M.S. Shahriar, B. Bernacki, H. Lamela-Rivera, S.P. Smith & S. Ezekiel, 41st Annual Symposium on Frequency Control, Philadelphia, 1987, p. 42

6.  R.N. Watts & C.E. Wieman, Opt. Lett. 11, 291 (1986); W.Ertmer & S. Penselin, Metrologia 22, 195 (1986).

## Figure Captions

Fig. 1    Schematic of Raman transition in cesium

Fig. 2    Experimental set up

Fig. 3    Laser linewidth measured by an optical spectrum analyzer

Fig. 4    Spectrum of : (a)  Modulated laser at 4.6 GHz

                        (b) Unmodulated laser

Fig. 5    Single zone cesium fluorescence when laser sidebands are scanned over 1-2 and 3-2 transitions simultaneously.

Fig. 6    (a) Expanded single zone Zeeman Raman transition in cesium

            (b) Single zone Zeeman components of Raman transition in cesium

Fig. 7    Ramsey fringes for a 15 cm zone separation

# Fig. 1    Schematic of Raman transition in cesium

Fig. 2    Experimental set up

Fig. 3    Laser linewidth measured by an optical spectrum analyzer

300 MHz

Fig. 4 Spectrum of : (a) Modulated laser at 4.6 GHz

(b) Unmodulated laser

45

Fig. 5   Single zone cesium fluorescence when laser sidebands are

scanned over 1-2 and also 3-2 transition

Fig. 7    Ramsey fringes for a 1 5 cm zone separation

Fig. 6    (a) Expanded single zone Zeeman Raman transition in cesium
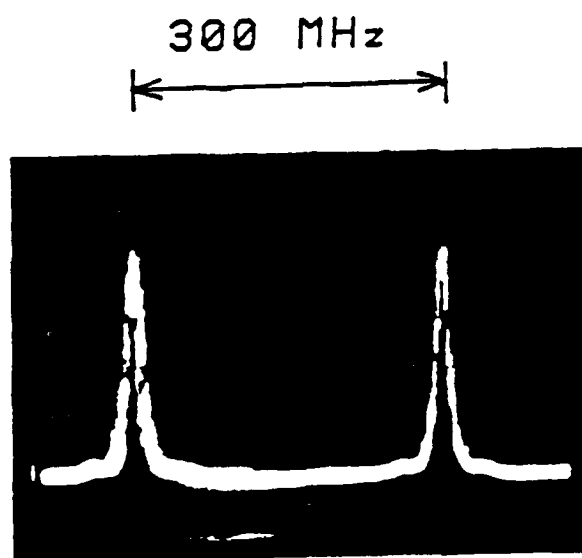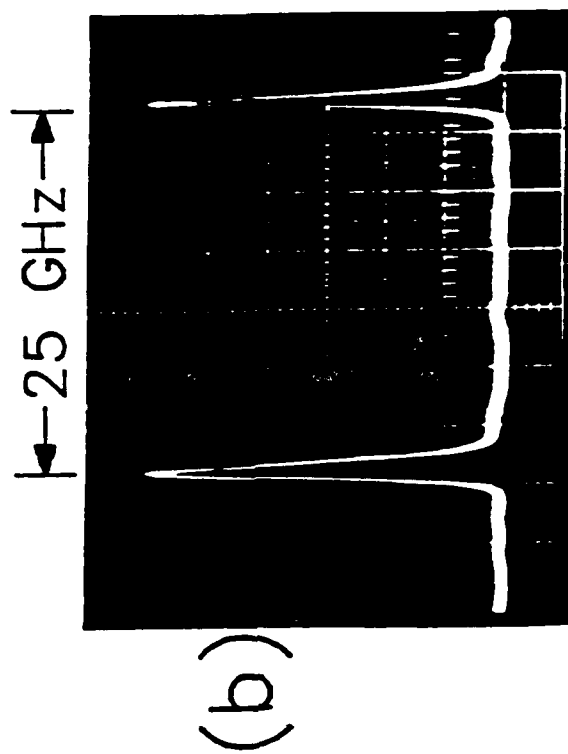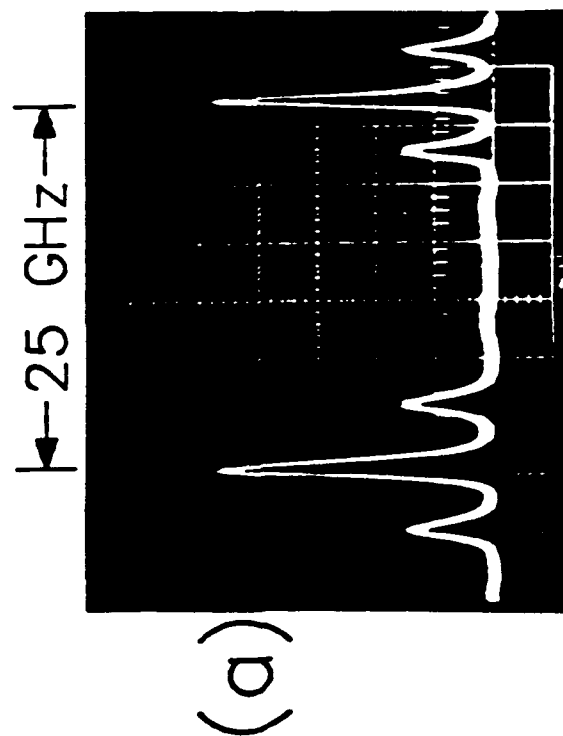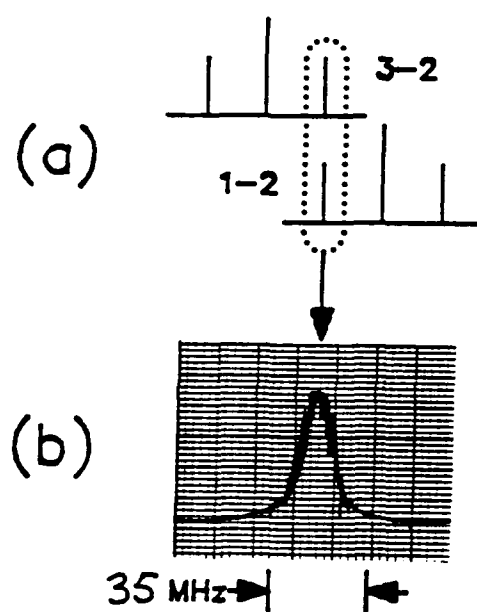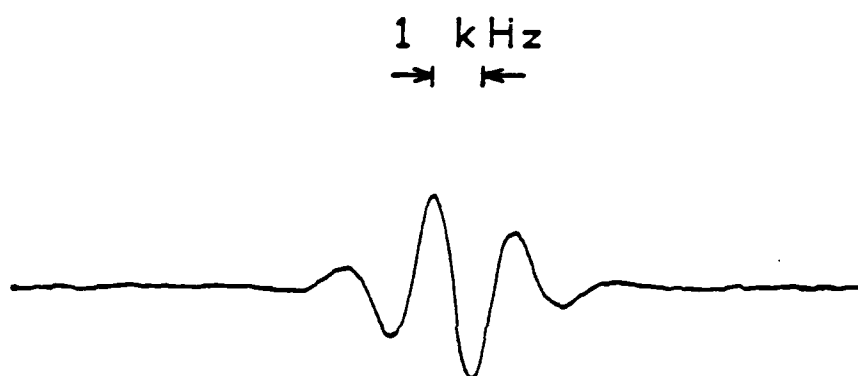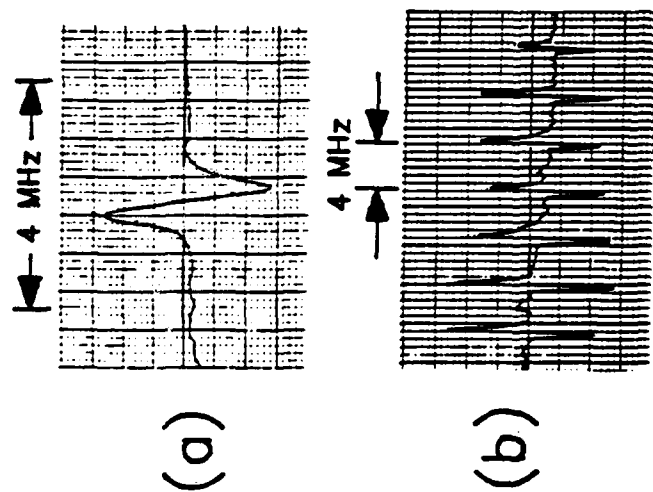
(b) Single zone Zeeman components of Raman transition in cesium

# Alignment-insensitive technique for wideband tuning of an unmodified semiconductor laser

B. E. Bernacki and P. R. Hemmer

Rome Air Development Center, Hanscom Air Force Base, Massachusetts 01731-5000

S. P. Smith and S. Ezekiel

Research Laboratory of Electronics, Massachusetts Institute of Technology, Cambridge, Massachusetts 02139

Using simple optical components and an unmodified commercial semiconductor laser, a frequency-selective self-aligning optical-feedback technique has been devised that allows a semiconductor laser to be tuned to and scanned about any optical frequency within the laser gain curve. This technique employs a graded-index rod lens cat's eye and an intracavity étalon.

Many applications, such as laser spectroscopy, optical pumping, and isotope separation, require a tunable narrow-linewidth source in the near infrared. Semiconductor lasers are an attractive alternative for these applications because of their relatively low cost, small size, and simplicity of operation. However, semiconductor lasers have had limited spectroscopic applications because of their inability to be tuned to arbitrary frequencies of interest within the laser gain curve. To alleviate this problem, several optical-feedback schemes have been devised that employ frequency-selective elements, such as gratings[1–5] or étalons,[6–11] in the feedback path. The most successful of these is discussed by Favre et al.,[1] who demonstrated continuous tuning of 15 nm with a linewidth of 20 kHz (deduced from beat spectrum). Wyatt and Devlin,[2] Whalen et al.,[3] DeLabachelerie and Cerez,[4] Sampei et al.,[5] and Voumard[6] have also demonstrated the ability to tune (discontinuously) to arbitrary frequencies within the laser gain curve with linewidths of 100 kHz or less. Of course, linewidth reduction without improved tuning characteristics has been achieved by others[11,12] using nonfrequency-selective feedback. However, all the optical-feedback techniques that demonstrate the ability to tune to arbitrary laser frequencies require the use of antireflection-coated lasers and, in addition, are highly sensitive to alignment of the external optics. These factors detract from the simplicity and low cost inherent in semiconductor lasers.

In this Letter, we describe a simple optical-feedback technique that permits an ordinary off-the-shelf semiconductor diode laser to be tuned to arbitrary frequencies within the laser gain curve. In addition, this method is not highly sensitive to optical misalignments. Briefly, a one-piece cat's-eye retroreflector serves as the feedback mirror, and a tilted intracavity solid étalon provides frequency selectivity. The use of a one-piece retroreflector contributes greatly to the simplicity of the technique because it eliminates the need for fine angular adjustment of the feedback mirror. The étalon, having approximately one fifth the optical thickness of the semiconductor laser, forces the laser to lase in the longitudinal mode of interest.

The basic laser feedback setup is shown in Fig. 1. The output of an off-the-shelf semiconductor laser is first collimated by a 0.22-pitch antireflection-coated plano-convex graded-index rod (GRINROD) lens and then filtered by the tilted solid étalon (optical thickness 0.15 mm, 80% reflectivity). Next, this light is reflected back into the laser by the uncoated rear surface[13] of a 0.25-pitch GRINROD lens mounted on a piezoelectric transducer (PZT) cylinder. This GRINROD lens serves as a one-piece cat's eye (i.e., retroreflector). Because of the self-aligning nature of the cat's-eye reflector, the external cavity consistently maintains its alignment so that there is no need to provide any adjustments for fine angular alignment.[14] The étalon passband is tuned by adjusting its tilt angle mechanically. Typical feedback light levels used in this experiment[15] are of the order of 0.25%, and the total cavity length is about 10 cm. For a 1-mm optical path length semiconductor laser cavity having 30% facet reflectivity, this results in a theoretical linewidth reduction factor of 55 using the expressions of Goldberg et al.[12] Of course, much greater linewidth reduction could be achieved with a longer external cavity.

The theory of single-mirror, low-level optical feedback is well known[12] but is reviewed here briefly. A semiconductor laser with a simple external-feedback mirror can be viewed as having an effective facet re-
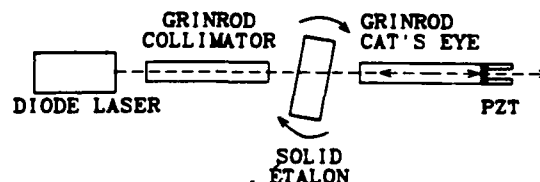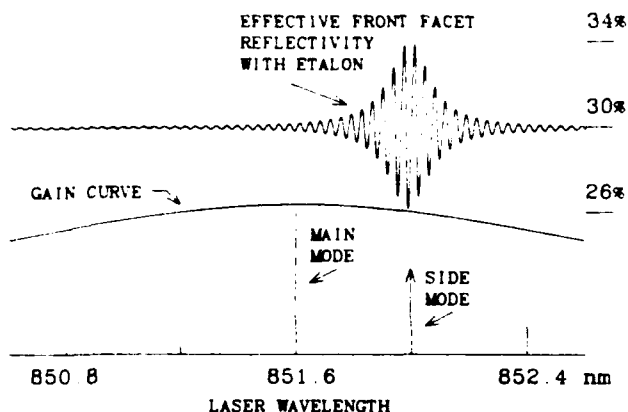


Fig. 1. Experimental setup.

Fig. 2. Laser longitudinal mode selection using an external reflector and étalon.

flectivity that varies sinusoidally with wavelength, where the period of the sine wave is determined by the free spectral range of the external cavity. With an intracavity étalon, this sinusoidally varying facet reflectivity is modulated by an envelope function that is derived from the étalon transmission, as illustrated in the upper portion of Fig. 2. For clarity, this figure corresponds to a 1-cm external cavity length, and the slope of the gain curve is exaggerated. If the étalon transmission is centered on any one of the possible laser modes (lower portion of Fig. 2), the laser is forced to oscillate only in that mode. Thus, by adjusting the passband of the étalon, the semiconductor laser can be forced to lase in a longitudinal mode that is different from the main mode. In fact, we have found that by appropriately choosing the finesse and free spectral range of the étalon, we are able to achieve lasing in any of five or six different longitudinal modes.

We now demonstrate the applicability of our technique to the excitation of a cesium resonance by employing a nominally 852-nm Ortel SL 300 laser. Figure 3 shows a series of traces obtained by ramping the laser current, $i$, from the threshold to the highest-rated current (40 mA) while monitoring the laser intensity after it passes through a cesium vapor cell. Figure 3(a) shows data obtained without optical feedback for a variety of different laser temperatures. As can be seen, the laser excites cesium efficiently only for one combination of temperature and current, i.e., the top trace. This is typical for several Ortel SL 300 lasers that we have tested, as well as for lasers from other manufacturers, and is a consequence of the well-known[16] discontinuous tuning characteristics of semiconductor lasers. In fact, for some nominally 852-nm lasers, it is not possible to excite the cesium resonance for any combination of current and temperature.

With our setup of Fig. 1, however, it is possible to force the laser to excite cesium at a variety of temperatures, as shown in Fig. 3(b). These cesium absorptions were obtained by simply tilting the étalon at each temperature until a strong cesium absorption was found.[17] These data illustrate that reliable tuning to an atomic resonance such as cesium is possible even though the laser may not excite the resonance without feedback. This is particularly important for practical

applications, since even lasers that excite an atomic resonance initially often fail to do so afterward as a consequence of aging.[18] The data in Fig. 3(b) also suggest that it is even possible to use a prechosen injection-current level (optical power output) and still be able to excite the cesium resonances. This is clearly a useful feature for design considerations.

Once the laser frequency has been selected, it is desirable in many applications to tune the laser continuously about the chosen frequency. As others have shown,[1,7,10] this can be done by changing the length of the external cavity, e.g., by using the PZT in Fig. 1. However, to achieve long-range continuous-frequency scans (greater than the external-cavity free spectral range) it is necessary to vary the external-cavity length and the injection current simultaneously.[19] This can be done either with an open loop or with a servo.[20] Figure 4 shows a typical open-loop scan of the cesium $D_2$ hyperfine components as a function of laser frequency. Note that this scan exceeds the 9.2-GHz separation of these lines.[21] In fact, the total scan range in this trace is about 20 GHz and is at present limited by
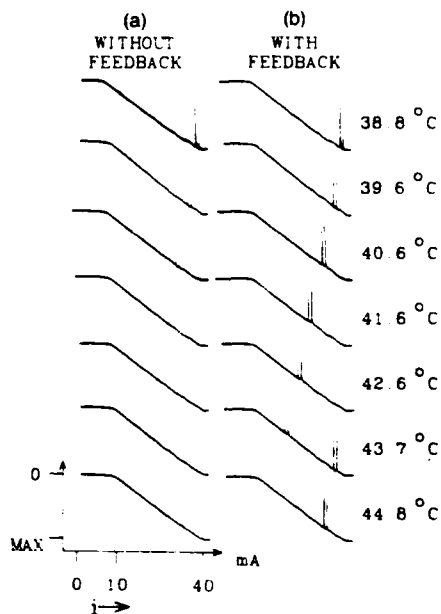


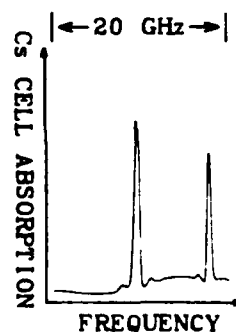Fig. 3. Absorption of cesium vapor cell versus laser current.



Fig. 4. Continuous laser frequency scan over cesium $D_2$ hyperfine components in a vapor cell. Total scan range is 20 GHz.

50

PZT travel. The important feature of these data is that they were obtained at temperature and injection-current levels for which the laser was unable to excite cesium without feedback.

Although the cesium resonances in a vapor cell have linewidths of the order of 1 GHz, many applications require that the laser have a much narrower linewidth. Measurements made with a 300-MHz free-spectral-range 2-MHz instrumental linewidth optical spectrum analyzer showed that the laser spectral linewidth remained less than 3 MHz (Ref. 22) over the entire 20-GHz scan of Fig. 4. This is consistent with the expected factor-of-55 linewidth reduction, mentioned earlier, for an Ortel SL 300 laser having a free-running linewidth of 125 MHz. Of course, the linewidth can be narrowed much further, if required, by using a longer external cavity, but at the expense of the continuous tuning range.

Finally, although the data in this Letter were obtained using Ortel SL 300 lasers, similar results were also obtained using Mitsubishi ML 2701 lasers.

In summary, we have demonstrated a novel, robust (phase- and alignment-insensitive) optical-feedback scheme that can be used to tune an unmodified off-the-shelf semiconductor laser to arbitrary frequencies within its gain curve. In addition, we also demonstrated repeatable continuous-frequency tuning of 20 GHz about the selected optical frequency, e.g., the cesium resonance. We plan to apply this technique to lasers from additional manufacturers and to extend the present 20-GHz continuous tuning range.

## References

1. F. Favre, D. Le Guen, J. C. Simon, and B. Landousies, Electron. Lett. **22**, 795 (1986).
2. R. Wyatt and W. J. Devlin, Electron. Lett. **19**, 110 (1983).
3. M. S. Whalen, K. L. Hall, D. M. Tennant, U. Koren, and G. Raybon, Electron. Lett. **22**, 313 (1987).
4. M. DeLabachelerie and P. Cerez, Opt. Commun. **55**, 174 (1985).
5. S. Sampei, H. Tsuchida, and M. Ohtsu, Jpn. J. Appl. Phys. **22**, 258 (1983).
6. C. Voumard, Opt. Lett. **1**, 61 (1977).
7. B. Dahmani, L. Hollberg, and R. Drullinger, Opt. Lett. **12**, 876 (1987).
8. A. G. Bulushev, E. M. Dianov, Yu. V. Gurov, O. G. Okhotnikov, A. M. Prokhorov, and B. P. Shurukhin, Opt. Lett. **13**, 19 (1988).
9. N. Dutta, E. Gordon, T. Shen, P. Anthony, and G. Zydzik, IEEE J. Quantum Electron. **QE-21**, 559 (1985).
10. A. M. Akul'shin, V. L. Velichanskii, M. V. Zverkov, A. S. Zibrov, V. V. Nikitin, O. G. Okhotnikov, V. A. Santenkov, N. V. Senkov, V. B. Taranenko, and E. K. Yurkin, Sov. Tech. Phys. Lett. **11**, 322 (1985).
11. F. Favre and D. Le Guen, IEEE J. Quantum Electron. **QE-21**, 1937 (1985), and references therein.
12. L. Goldberg, H. F. Taylor, A. Dandridge, J. F. Weller, and R. O. Miles, IEEE J. Quantum Electron **QE-18**, 555 (1982).
13. The front surface of the GRINROD cat's eye in our setup is antireflection coated. However, this is not essential, since the front surface reflection is highly alignment sensitive and can easily be deflected away from the laser.
14. Theoretically, a cat's-eye retroreflector merely trades angular sensitivity for transverse positional sensitivity. However, experimentally, for a 1-mm-diameter (FWHM) semiconductor laser beam and a 2-mm-diameter GRINROD cat's eye, it is found that the feedback light level remains relatively constant when the transmitted portion of the laser beam merely passes unobstructed through the GRINROD.
15. Feedback light level was controlled by using either a variable attenuator or a rotating polarizer or by simply translating the 2-mm GRINROD cat's eye so as partially to eclipse the feedback light.
16. G. P. Agrawal and N. K. Dutta, *Long Wavelength Semiconductor Lasers* (Van Nostrand Reinhold, New York, 1986).
17. Here it should be emphasized that the data in Fig. 3 do not correspond to a continuous laser frequency scan but merely demonstrate the ability to excite cesium over a broad temperature or injection-current range.
18. M. Ohtsu, M. Hashimoto, and H. Ozawa, in *Proceedings of the 39th Annual Frequency Symposium* (Institute of Electrical and Electronics Engineers, New York, 1985), p. 43.
19. It was not necessary to adjust the étalon tilt angle for the continuous scan ranges used in our experiment.
20. We constructed a servo for this purpose by modulating the laser current and demodulating the laser output power to produce an error signal. However, the laser current modulation produced approximately 100 MHz of laser frequency modulation, which is unacceptable for some applications.
21. The additional structure visible in the data of Fig. 4 results from adjacent side modes of the external cavity, 1.5 GHz to either side of the main mode. These side modes typically arise for feedback light levels slightly greater than optimum and can of course be made smaller, at the expense of linewidth, by attenuating the optical-feedback light.
22. In addition, there was approximately 15 MHz of laser frequency jitter present, owing to acoustically induced fluctuations in the external-cavity length.

# STUDY OF SEVERAL ERROR SOURCES IN A LASER RAMAN CLOCK

P.R. Hemmer*, V.D. Natoli, M.S. Shahriar, B. Bernacki*,

H. Lamela-Rivera, S.P. Smith and S. Ezekiel

Research Laboratory of Electronics

Massachusetts Institute of Technology

Cambridge, MA 02139

### Abstract

We are investigating the development of a cesium clock using a laser excited resonance Raman interaction in place of direct microwave excitation. Such a scheme, employing only semiconductor laser excitation and exploiting fiber optic and integrated optic technology together with a simple atomic beam design, may lead to the development of smaller, lighter and perhaps cheaper atomic clocks. So far, we have been studying a sodium Raman clock which consists of a sodium atomic beam, a dye laser, and an acousto-optic frequency shifter, used for the generation of the second laser frequency. Recent performance showed a stability of $1 \times 10^{-11}$ for a 5000 second averaging time. This compares favorably with commercial cesium clocks, when difference in atom transit time and transition frequency are taken into consideration. In this paper, we describe the results of a study of long term error sources unique to the Raman clock, which include: laser beam misalignment effects, errors caused by the laser frequency being slightly off-resonance with the intermediate state, laser intensity effects, and so on.

## I. Introduction and Background

We have been investigating the performance of a clock based on laser induced resonance Raman transition in an atomic beam to determine the feasibility of such a scheme and to demonstrate any possible advantages over conventional microwave excited clocks. Although we have been conducting our experiments so far using a sodium atomic beam and dye lasers, this Raman technique is also applicable to a cesium atomic beam employing semiconductor laser excitation and may lead to the development of smaller, lighter and less expensive cesium beam clocks. Among the advantages of such a clock over a conventional cesium clock are the absence of state selection magnets and a microwave cavity, and that all alignments can be made using optics external to the vacuum system.
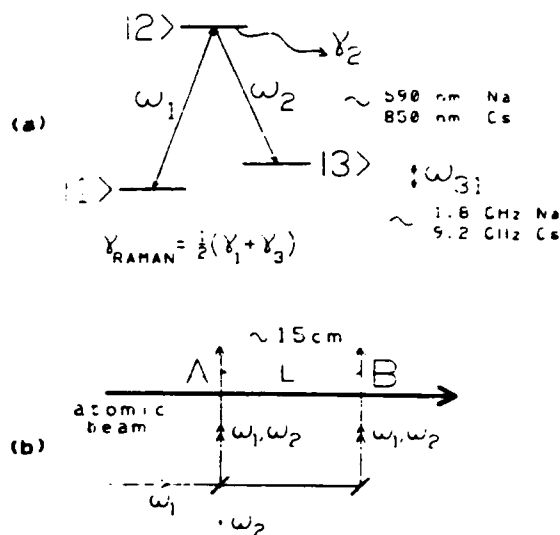


Fig. 1

(a) Schematic of laser induced resonance Raman interaction.
(b) Schematic of separated field excitation.

The stimulated resonance Raman interaction is illustrated using the three level system in Fig. 1(a). Briefly, Raman transitions are induced between states 1 and 3 using two laser fields, at frequencies $\omega_1$ and $\omega_2$, simultaneously resonant with the intermediate state 2. Earlier studies [1,2] show that, for copropagating laser fields interacting with an atomic beam at right angles, the Raman linewidth is determined by the widths of states 1 and 3 only. State 2 greatly enhances the transition probability, but does not contribute to the linewidth. Thus, for long lived states 1 and 3, the Raman linewidth becomes transit time limited, just as for direct microwave excitation.

* Rome Air Development Center,
Hanscom AFB, Bedford, MA 01731

52

To obtain a very small transit time linewidth we use Ramsey's method of separated oscillatory fields [3], as illustrated in Fig. 1(b), in analogy with conventional microwave techniques. In separated field excitation, the atom-field superposition states, excited in zones A and B by the two-photon Raman interaction, interfere quantum mechanically. Thus, the resulting interference fringes, as in the microwave case, have frequency spacings which are characteristic of the transit time between the interaction zones.

II. Experimental Setup

The experimental setup [4,5] used to demonstrate Raman clock applications is illustrated in Fig. 2. The laser at frequency $\omega_1$ is obtained from a single mode dye laser locked to the sodium $D_1$ transition, using fluorescence from the atomic beam. The laser field at frequency $\omega_2$ is generated directly from that at $\omega_1$ by an acoustic-optic frequency shifter, driven by a quartz stabilized microwave oscillator near the 1772 MHz sodium hyperfine transition frequency. This greatly reduces the effects of laser jitter by correlating the frequency jitters [2] of $\omega_1$ and $\omega_2$ so as to produce a highly stable difference frequency. After leaving the A/O, the laser beams at $\omega_1$ and $\omega_2$ are combined in a single mode fiber, to ensure copropagation, before exciting the atomic beam at the two interaction zones, labeled A and B in Fig. 2.

A magnetic field is applied externally to separate out the different m-levels and right circularly polarized light is used. The m=0 and $\Delta$m=0 Raman transition is then selected so that the clock frequency be insensitive to external magnetic field variations to first order.
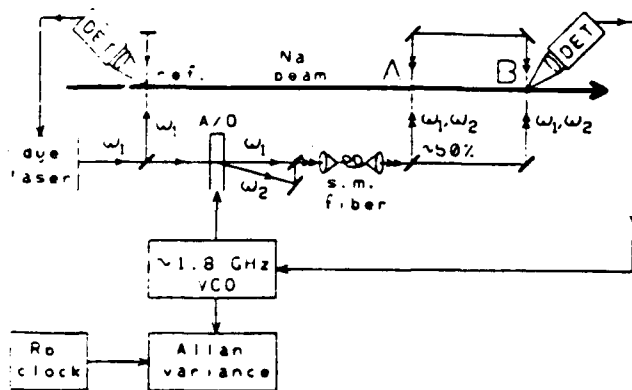
Typical Raman/Ramsey fringes appear in Fig. 3(a). These fringes are observed by monitoring the fluorescence induced in zone B while scanning the microwave frequency with $\omega_1$ locked to the $D_1$ transition. The central fringe has a width of about 2.6 KHz (FWHM) which is consistent with the transit time for the 15 cm interaction zone separation.

To stabilize the frequency of a microwave oscillator to the central fringe in Fig. 3(a), a discriminant is needed. This discriminant, shown in Fig. 3(b), is obtained by frequency modulating the microwave source at a rate $f_m$ = 610 Hz and demodulating the zone B fluorescence signal with a lock-in amplifier. The output of the lock-in amplifier is then used in a feedback loop to hold the microwave oscillator frequency at the central zero of the discriminant. The stability of this oscillator is measured by comparing it with a commercial rubidium clock.
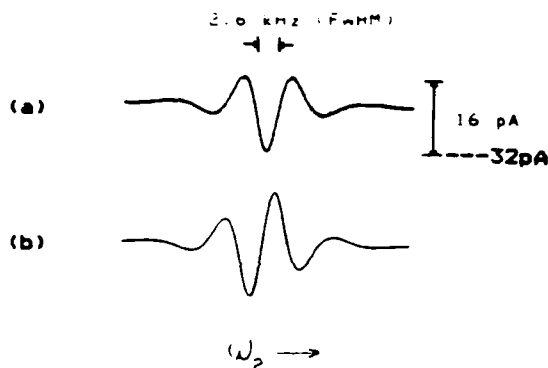


Fig. 3

(a) Typical Raman/Ramsey fringe lineshape for a 15 cm interaction zone separation. Photomultiplier photocathode current levels as shown.
(b) Discriminant obtained using frequency modulation.



Fig. 2

Schematic of the experimental Raman clock setup.

III. Clock Performance

Figure 4 shows a plot of the measured fractional frequency stability of the stabilized microwave oscillator, $\sigma_y(\tau)$, as a function of averaging time, $\tau$. For $\tau$ = 5000 secs., the stability is about $1 \times 10^{-11}$. The data in this plot is very close to the predicted shot noise limit, shown by the upper dashed line. The lower dashed line in the figure is the projected stability expected if cesium were used in place of sodium, the difference being the result of the larger transition frequency and mass of cesium. As can be seen, the projected cesium results compare favorably with commercial cesium clocks.

53

Fig. 4

Fractional frequency stability vs.
averaging time for the sodium Raman clock.



Fig. 5

(a) Schematic illustrating correlated laser
    detuning $\delta$.
(b) Schematic of experimental technique for
    generating $\delta$.
(c) Plot of clock error as a function of $\delta$.

## IV. Frequency Error Sources

We have been studying potential sources of error that
can cause long term frequency drifts in the Raman process.
Some error sources are similar to those of microwave clocks.
These include the effects of path length phase shift, magnetic
field, background slope, atomic beam misalignment,
second-order Doppler, as well as errors due to electronics.
In addition, there are errors unique to the Raman clock, such
as those caused by laser frequency detuning, laser intensity
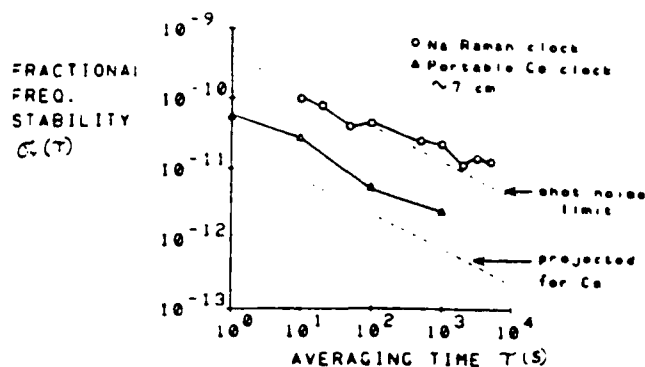changes, laser beam misalignment, optical atomic recoil, the
presence of nearby hyperfine levels, and other smaller
effects.

Here we will consider only error sources that are unique
to the Raman clock.

### (a) Correlated laser frequency detuning effects

Frequency errors can arise when $\omega_1$ and $\omega_2$ are
off-resonance (by the same amount) with state 2, as shown
in Fig. 5(a), where $\delta$ is the correlated detuning. The typical
effect of $\delta$ on clock frequency error is shown in Fig. 5(c). To
scan $\delta$, the reference beam in Fig. 5(b) is frequency shifted
with an A/O, so that $\omega_1$ and $\omega_2$ can be tuned with reference to
the $D_1$ resonance. As can be seen, the clock frequency
depends strongly on correlated detuning. However, for $\delta = 0$
this dependence is small. For the data shown the slope of
clock error near $\delta = 0$ is 0.43 Hz for a detuning of 1% of the $D_1$
linewidth (equivalent to a fractional error of $2.4 \times 10^{-10}$ for the
same amount of detuning).

However, this slope depends on the laser intensity in
the interaction zones as well as the intensity in the reference
beam. For example, Fig. 6 shows the effect of interaction
zone intensity on this slope. Here, clock error as a function
of $\delta$ is plotted for three different interaction zone intensities.
As can be seen, the slope is smallest for the interaction zone
intensity of 0.8 mW/cm$^2$. Similarly, we studied the
dependence of this slope on the reference beam intensity.
The minimum slope achieved so far is, in fractional error, 2.4
$\times 10^{-11}$ for a detuning of 1% of the $D_1$ linewidth and it should
be possible to reduce this further.

Laser misalignment also causes clock errors indirectly. For example, vertical misalignment causes effective laser intensity changes, as shown in Fig. 7(a), because of the translation of the Gaussian profile of the laser beam with respect to the atomic beam. Horizontal misalignment causes both translational and angular effects, as shown in Fig. 7(b). The angular misalignment creates effective correlated laser detuning due to the Doppler effect. The translational misalignment generates intensity error due to the translation of the laser beam relative to the detector. Misalignment in general can also cause imperfections in the standing waves that are used to reduce the effects of path length phase shifts. Imperfect standing waves cause errors because of changes in effective intensity as well as in path length phase.

To experimentally measure laser misalignment effects, we first find an optimum operating point at which laser detuning, laser intensity changes and path length phase shifts have minimal effects on clock frequency. Path length phase shift errors are minimized by adjusting the path lengths so that the clock frequency is the same for standing and travelling wave excitations. Around this optimum operating point we found that errors due to translations of the beams are much larger than those due to angular misalignments. Typically, the fractional error due to beam translation is about $3 \times 10^{-11}$ for a 0.1 mm beam displacement.
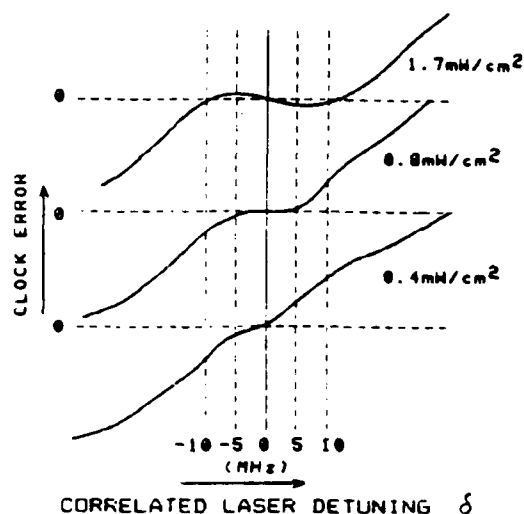


CORRELATED LASER DETUNING $\delta$

Fig. 6

Plots of clock error as a function of correlated laser detuning $\delta$, for three different interaction zone intensities.

## (b) Laser intensity effects

Frequency errors can also arise when the laser intensity changes in $\omega_1, \omega_2$ and the reference beam, together or separately. For $\delta = 0$, the predicted intensity induced errors are due to any fluorescence background slope, the presence of nearby hyperfine levels, optical atomic recoil, and so on. However, if correlated detuning $\delta$ is nonzero, then the amount of intensity induced error is determined primarily by the amount of detuning.

To illustrate this strong dependence of intensity induced error on detuning, we refer to Fig. 6 again. As can be seen, clock error is least sensitive to changes in intensity when detuning is nearly zero. We can find an optimum operating point by adjusting the amount of detuning. Around such a point the minimum slope achieved so far is $2.5 \times 10^{-12}$ fractional error for 1% change in intensity.

Efforts are underway to study the individual causes of intensity induced errors mentioned above. For example, to determine the effect of nearby hyperfine levels we propose to study other transitions where this effect is expected to be different in magnitude.
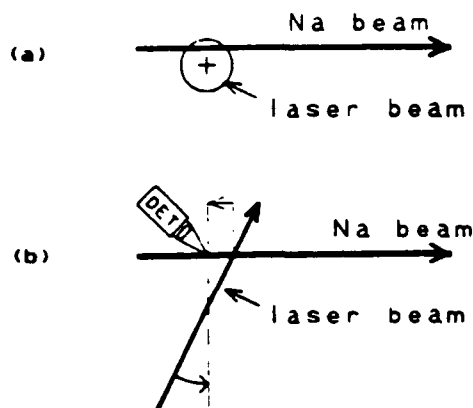


Fig. 7

(a) Schematic illustrating how vertical misalignment causes effective laser intensity changes.
(b) Schematic illustrating how horizontal misalignment changes correlated detuning through angular effects and effective intensity through translational effects.

## V. Other Error Sources

Potential frequency-error sources that have not yet been studied include the effects of fluorescence from the interaction zones, the second-order Doppler shifts, limitations of single mode fibers, and so on.

## VI. Future Work

As mentioned earlier, one of the more promising applications of the Raman technique is to develop a cesium atomic beam Raman clock, using semiconductor lasers. Such a clock, in which the two frequencies are intensity modulation sidebands, is nearing completion. As projected in Fig. 4, use of cesium is expected to increase the stability by a factor of 16. Also, this setup will have a more compact, recirculating cesium oven, with an atom throughput much larger than that of our present setup. Coupled with planned improvements in fluorescence collection efficiency, this is expected to enhance the signal to noise ratio considerably. With all the beams, atomic and laser, on the same table, misalignment will be greatly reduced. Also, the new beam will allow for much better shielding and control of magnetic fields. All these are expected to enhance our ability to study the remaining error sources with higher resolution.

We are also considering the attractive possibility of extending the resonance Raman technique into the mm-wave region of the spectrum. At these much higher transition frequencies, it may be possible to achieve better clock stabilities and many of the experimental problems associated with exciting mm-wave transitions in an atomic beam could be avoided. Finally, the Raman technique can also be readily applied to slowed or trapped atoms, possibly without greatly increasing the complexity of the experimental setup, since many of these techniques already make extensive use of resonant light.

## Acknowledgements

## References

[1] J.E. Thomas, S. Ezekiel, C.C. Leiby, Jr., R.H. Picard and C.R. Willis, "Ultrahigh-resolution spectroscopy and frequency standards in the microwave and far infrared regions using optical lasers," Opt. Lett. 6, 298 (1981) and references therein.

[2] J.E. Thomas, P.R. Hemmer, S. Ezekiel, C.C. Leiby, Jr., R.H. Picard and C.R. Willis, "Observation of Ramsey fringes using a stimulated resonance Raman transition in a sodium atomic beam," Phys. Rev. Lett. 48, 867 (1982).

[3] N.F. Ramsey, Molecular Beams (Oxford U. Press, London, 1963).

[4] P.R. Hemmer, S. Ezekiel and C.C. Leiby, Jr., "Stabilization of a microwave oscillator using a resonance Raman transition in a sodium beam," Opt. Lett. 8, 440 (1983).

[5] P.R. Hemmer, G.P. Ontai, and S. Ezekiel, "Precision studies of stimulated-resonance Raman interactions in an atomic beam," Journal of OSA, vol. 3 (1986).

# Ac Stark shifts in a two-zone Raman interaction

P. R. Hemmer

*Rome Air Development Center, Hanscom Air Force Base, Bedford, Massachusetts 01731*

M. S. Shahriar, V. D. Natoli,* and S. Ezekiel

*Research Laboratory of Electronics, Massachusetts Institute of Technology, Cambridge, Massachusetts 02139*

We have measured the ac Stark effect in a two-zone stimulated Raman interaction in a sodium atomic beam. In addition, we have derived simple theoretical expressions for the ac Stark shift, based on a closed three-level system, in the $\Lambda$ configuration, and have achieved qualitative agreement with the data. In particular, the magnitude and sense of the ac Stark shifts are found to depend on laser intensities as well as on the initial populations of the two low-lying levels of the $\Lambda$ configuration. Specifically, the observed ac Stark shifts are smaller for larger laser intensities and also for smaller initial population differences between the two low-lying levels. The ac Stark effect must be considered for many potential applications of the Raman effect, such as a Raman clock. In this connection, we have identified conditions for the reduction of the ac Stark shift in our sodium Raman clock.

## INTRODUCTION AND BACKGROUND

Much recent work, both theoretical and experimental, has been performed to identify potential applications of the stimulated Raman interaction. These include application to the study of fundamental atom–field interactions,[1-3] collisional diffusion,[4] Raman lasers,[5] and new time and frequency standards.[6-8] For all these applications, and especially for time and frequency standards, it is important to understand thoroughly all sources of line-shape asymmetries and level shifts. The ac Stark effect is therefore of special interest because of its fundamental nature and because it produces line-shape asymmetries and level shifts that can be significant under certain conditions.

In this paper we report the results of our experimental and theoretical studies of the ac Stark effect in a two-zone stimulated Raman interaction, using a sodium atomic beam. The two-zone excitation scheme is used because it is important for potential clock applications and because it provides unique physical insights into the nature of the ac Stark effect in the stimulated Raman interaction. Previous theoretical treatments[2,8] of the ac Stark shifts in a Raman interaction are confined primarily to single-zone excitation and do not include the effects of saturation.

We will begin by presenting data showing the ac Stark shift in the Raman two-zone excitation scheme as a function of laser detuning for various experimental conditions, for example, different laser intensities and initial atomic state populations. This is followed by a brief derivation of simple, closed-form theoretical expressions for the Raman ac Stark shift in the two-zone excitation scheme, assuming an ideal, closed three-level system. Agreement of these simple calculations with the data is then illustrated for various cases. Next, the simple theory is augmented to account for the fact that more than three levels are involved in the interaction, and the modified theory shows improved agreement with the data. Finally, it is shown that proper choice

of experimental conditions can reduce the ac Stark shift to levels acceptable for potential clock applications.[7]

The stimulated Raman interaction is illustrated schematically with the three-level system in Fig. 1(a). Briefly, Raman transitions are induced between states 1 and 3 by using two laser fields, at frequencies $\omega_1$ and $\omega_2$, simultaneously resonant with the intermediate state 2. Experimentally, if $\omega_1$ is held fixed at the 1–2 transition frequency and $\omega_2 - \omega_1$ is scanned over the 3–2 transition, a fluorescence line shape such as the one shown in Fig. 1(b) results. Here, the Raman interaction appears as a dip in fluorescence (trapped state formation[1,2]) that in this case occurs at the center of the $\gamma_2$ wide 3–2 transition. Earlier studies[3,4,6] show that, for copropagating laser fields interacting with an atomic beam at right angles, the Raman linewidth is determined by the widths of states 1 and 3 only. State 2 greatly enhances the transition probability but does not contribute to the linewidth. Laser jitter effects are greatly reduced by generating both frequencies from the same laser with an acousto-optic frequency shifter, driven by a microwave oscillator. Thus, for long-lived states 1 and 3, the Raman linewidth becomes transit-time limited, just as for direct microwave excitation.

Ac Stark shifts in the Raman system arise when the laser fields are tuned off resonance with the intermediate state. This is illustrated in Fig. 1(c) in the case when both laser frequencies are detuned by the same amount (common-mode detuning). Such detunings produce asymmetric Raman line shapes, as shown by the data of Fig. 1(d). These asymmetries are manifestations of the ac Stark effect (light shift) in the single-zone Raman interaction.

Two-zone excitation of the stimulated Raman interaction is illustrated in Fig. 2(a). This scheme is analogous to Ramsey's method of separated-microwave-field excitation[9] in an atomic beam. Briefly, in separated-field excitation long-lived atomic polarizations are induced in the two interaction zones. These polarizations interfere and produce fringes

(a)                          (c)
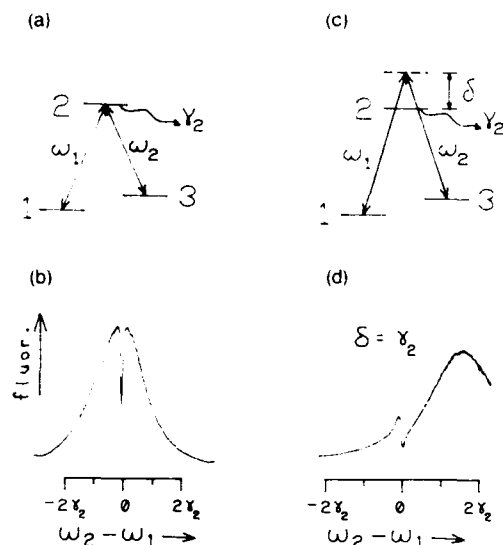


(b)                          (d)



Fig. 1.   (a) Schematic of stimulated resonance Raman interaction, (b) single-zone resonance Raman line shape, (c) schematic of off-resonance Raman interaction, and (d) single-zone off-resonance Raman line shape.

whose widths (measured in terms of laser difference frequency) are characteristic of the atom transit time between the two interaction zones. Figure 2(b) shows a typical Raman–Ramsey fringe line shape observed experimentally by monitoring the zone B fluorescence as the laser difference

frequency is scanned. The central fringe has a width of ~2.3 kHz (FWHM), which is consistent with the transit time for the 15-cm interaction-zone separation and the thermal velocity of $\sqrt{2kT/M}$ = 7 × 10⁴ cm/sec for a sodium beam produced by a 400°C oven. As is well known,[3] the envelope function for these fringes is determined by velocity averaging, as illustrated in Fig. 2(c). The dotted curves in this figure are single-velocity fringes, which are pure cosines, and the solid curve is the velocity-averaged fringe pattern.

As will be shown below, ac Stark shifts in the two-zone Raman interaction can be expressed as a phase shift in the cosine function describing the Ramsey fringe. Such Ramsey-fringe phase shifts are well known from microwave studies and in this connection arise when the microwave excitation fields in the two excitation zones are not in phase.[3] These Ramsey-fringe phase shifts result in frequency shifts of the central-fringe minima and also produce line-shape asymmetries when velocity averaging is included. This is illustrated in Fig. 2(d) for the case of a constant $\pi/2$ phase shift.

Figure 3 shows experimentally observed Raman–Ramsey fringes that are similar in appearance to the phase-shifted fringes of Fig. 2(d). All three data in Fig. 3 were obtained for a common-mode laser detuning of $\delta = 0.8\gamma_2$ but different initial atomic state populations. Figure 3(a) corresponds to the case when all the atoms are initially placed in state 1, by optical pumping to be described below. Figure 3(b) corresponds to initially equal state 1 and 3 populations, and Fig.
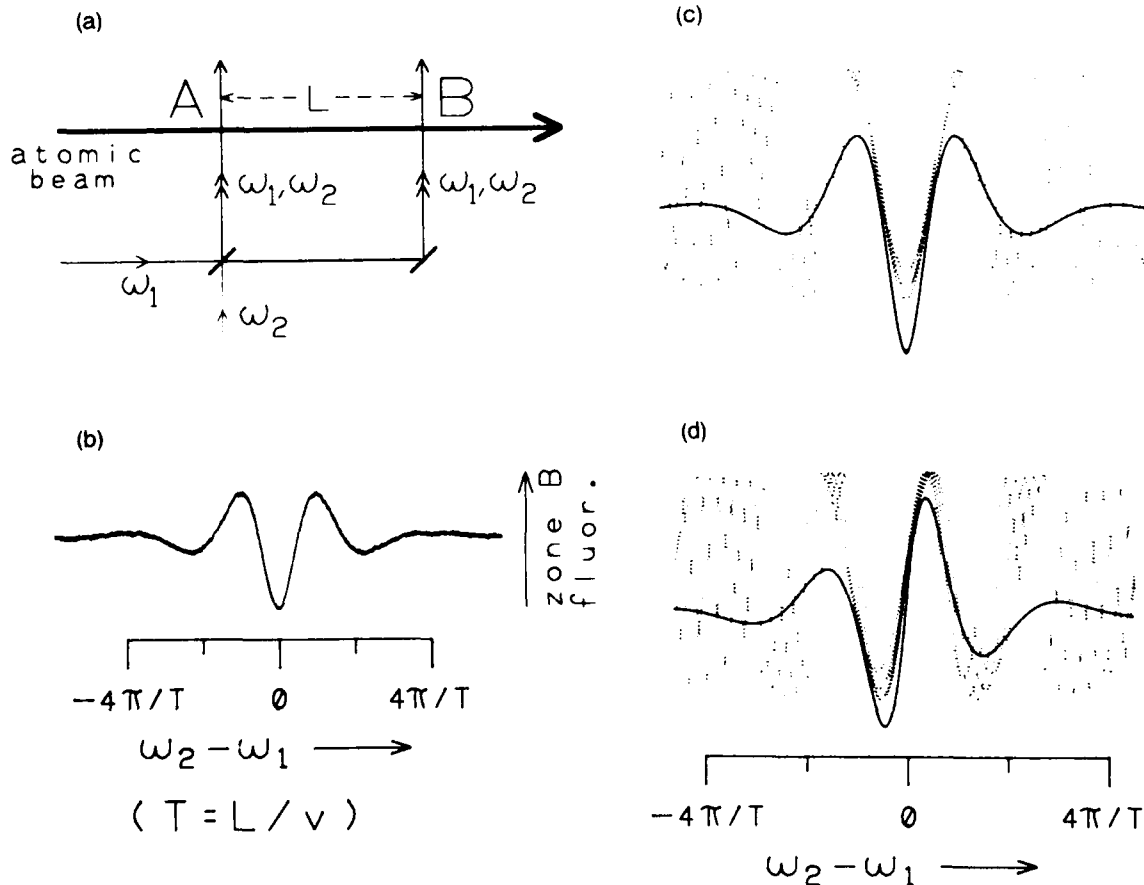
(a)



(c)



(b)



(d)



Fig. 2.   (a) Schematic of separated-field Raman excitation, (b) two-zone Ramsey-fringe line shape observed in zone B fluorescence, (c) theoretical fringe shape resulting from velocity averaging, and (d) theoretical velocity-averaged fringe shape for $\pi/2$ phase-shifted fringes.
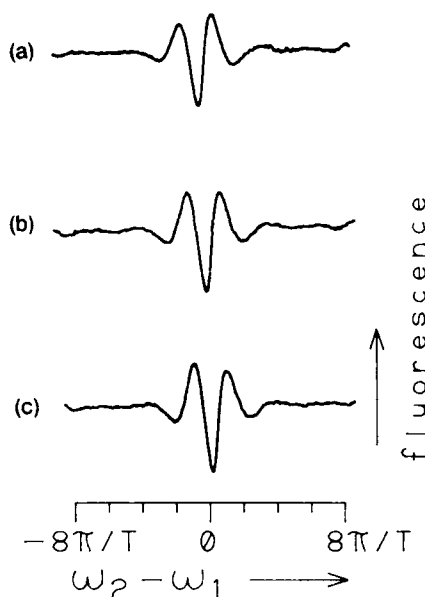
Fig. 3.  Observed Ramsey-fringe asymmetries for a fixed common-mode detuning of $\delta = 0.8\gamma_2$.  Initial populations:  (a) $\rho_{11}{}^0 = N$, $\rho_{33}{}^0 = 0$; (b) $\rho_{11}{}^0 = \rho_{33}{}^0 = N/2$; (c) $\rho_{11}{}^0 = 0$, $\rho_{33}{}^0 = N$.

3(c) to all atoms initially in state 3.  As can be seen, the magnitude as well as the sense of the ac-Stark-produced asymmetry depends on the initial atomic state populations.  As expected, the magnitude and sense of the ac-Stark-induced asymmetry also depend on the common-mode laser detuning (not shown) for fixed initial atomic state populations.  These observations will be quantified below.

## EXPERIMENT

For most applications, specifically those related to clocks, it is the frequency shift in the Ramsey-fringe central minimum, rather than the detail of the asymmetrical line shape, that is of immediate interest.  Therefore in our experiment we concentrate on observing the frequency shift of the cen-

tral minimum as a function of various parameters, for example, common-mode laser detuning, initial atomic state populations, and laser intensity.  Experimentally, this is accomplished by locking the laser difference frequency to the central Ramsey-fringe minimum, using a servo, and recording the stabilized difference frequency as different parameters are varied.

Figure 4 schematically illustrates the experimental setup used to measure two-zone Raman ac Stark shifts as a function of common-mode laser detuning in a sodium atomic beam.  As shown, the laser field at frequency $\omega_1$ (590 nm) is the output of a cw dye laser having 1 MHz of frequency jitter.  The field at frequency $\omega_2$ is generated from that at $\omega_1$ by using an acousto-optic modulator, A/O(1), driven by a voltage-controlled oscillator, VCO(1).  VCO(1) can be tuned over the 1–3 Raman transition frequency (1772 MHz).  The laser fields at $\omega_1$ and $\omega_2$ are combined by using a beam splitter before exciting the atomic beam at zones A and B, as shown.  Another portion of the laser beam at $\omega_1$ is shifted by a second modulator, A/O(2) (actually a pair of modulators), so that the shifted laser frequency $\omega_1 + \delta$ can be tuned both above and below $\omega_1$.  This shifted laser frequency is then locked to the 1–2 transition with fluorescence produced in the reference interaction zone (REF), as shown.  By using this scheme, $\omega_1$ and $\omega_2$ are simultaneously scanned over the 1–2 and 3–2 transitions, respectively (common mode scan), by simply tuning VCO(2).  The laser in the reference zone is also used to adjust the initial state 1 and 3 populations by means of optical pumping.  In this experiment, levels 1 and 3 are the $F = 1$ and $F = 2$ hyperfine sublevels, respectively, of the $^2S_{1/2}$ ground state, and state 2 is the $F = 2$ sublevel of the $^2P_{1/2}$ state.  The laser beams in zones A and B are right-circularly polarized, while the beam in the reference zone is linearly polarized.  A magnetic field is applied parallel to the **k** vectors of the laser fields.  Thus only $\sigma^+$ excitations are allowed in the interaction zones (and both $\sigma^+$ and $\sigma^-$ in the reference zone).

Figure 5 shows a set of data obtained with this experimental setup.  Each trace is the observed two-zone ac Stark shift
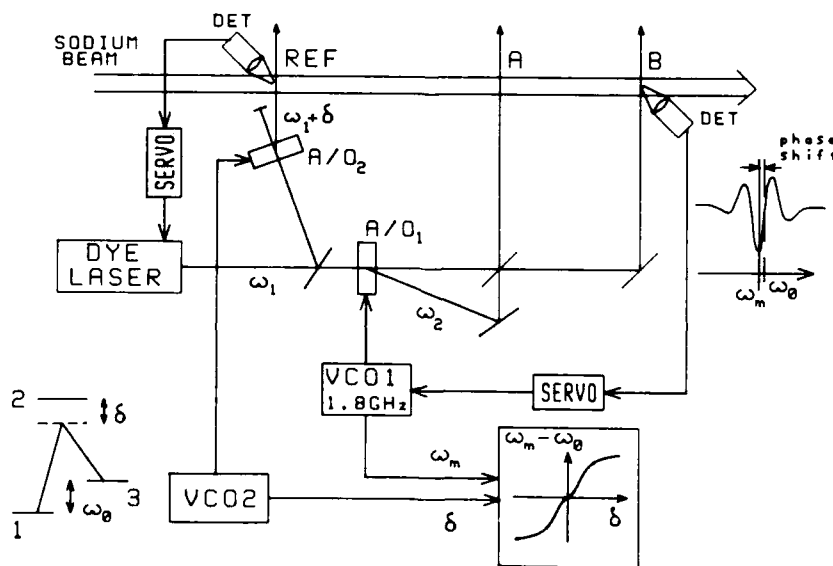


Fig. 4.  Schematic of experimental setup for measuring the ac Stark shift as a function of common-mode laser detuning.  DET's, detectors.
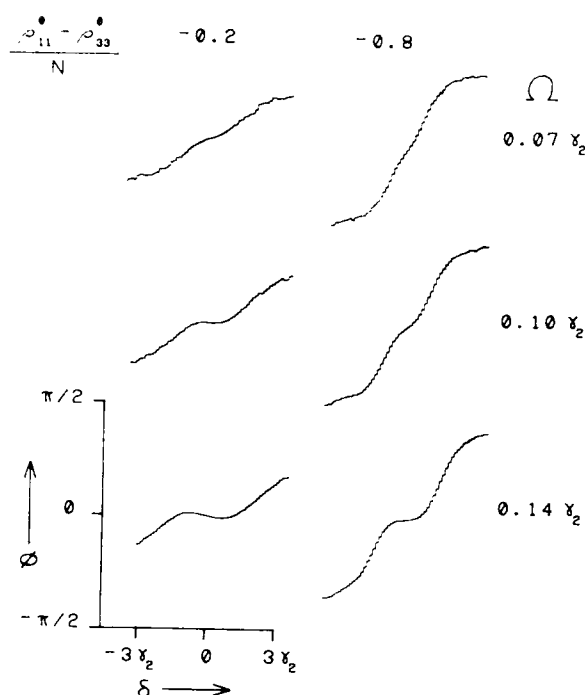
Fig. 5.   Data showing the ac Stark shift as a function of common-mode laser detuning, for several combinations of laser intensity and initial populations, as labeled.

as a function of common-mode laser detuning, $\delta$, where $\delta$ varies from $-3.2\gamma_2$ to $+3.2\gamma_2$, a total range of $\sim 6.4$ times the state 2 linewidth. The values of average[10] laser intensity (at zones A and B) and the initial atomic state population differences are as indicated. To simplify comparison with theory, the observed ac Stark shifts are expressed in units of Ramsey-fringe phase shift, where a $\pi/2$ phase shift corresponds to a frequency shift of the central fringe minimum by one fourth of the 2.3-kHz fringe spacing.

Examination of the data in Fig. 5 shows that, at low laser intensities (top row), the ac Stark shift is nearly linear with laser detuning, for detunings less than $2\gamma_2$. The slope is determined by the initial state 1 and 3 populations, where larger population differences produce larger ac Stark shifts. In contrast, for higher laser intensities in zones A and B (middle and bottom rows), the ac Stark shift is smaller, near zero laser detuning. However, for larger laser detunings (greater than $\sim 2\gamma_2$), the ac Stark shift is once again determined primarily by initial state 1 and 3 populations, as in the low-intensity data. In all cases, the ac Stark shift never exceeds $\pi/2$.

## THEORY

To calculate the Ramsey-fringe line shape (and ac Stark shifts) that are observed in the zone B fluorescence, the time-dependent density-matrix equations are the natural choice. These density-matrix equations have been derived by many authors,[2] and the procedure will only be reviewed here. The relevant density-matrix equations are as follows:

$$\dot{\rho}_{11} = - (\tfrac{1}{2}i\Omega_1\alpha_{12} + \text{c.c.}) + \Gamma_{21}\rho_{22}, \tag{1a}$$

$$\dot{\rho}_{22} = (\tfrac{1}{2}i\Omega_1\alpha_{12} + \text{c.c.}) + (\tfrac{1}{2}i\Omega_2\alpha_{32} + \text{c.c.}) - \gamma_2\rho_{22}, \tag{1b}$$

$$\dot{\rho}_{33} = - (\tfrac{1}{2}i\Omega_2\alpha_{32} + \text{c.c.}) + \Gamma_{23}\rho_{22}, \tag{1c}$$

$$\dot{\alpha}_{12} = \tfrac{1}{2}i\Omega_1{}^*(\rho_{22} - \rho_{11}) - \tfrac{1}{2}i\Omega_2{}^*\alpha_{13} - (\tfrac{1}{2}\gamma_2 + i\delta_1)\alpha_{12}, \tag{1d}$$

$$\dot{\alpha}_{32} = \tfrac{1}{2}i\Omega_2{}^*(\rho_{22} - \rho_{33}) - \tfrac{1}{2}i\Omega_1{}^*\alpha_{13}{}^* - (\tfrac{1}{2}\gamma_2 + i\delta_2)\alpha_{32}, \tag{1e}$$

$$\dot{\alpha}_{13} = \tfrac{1}{2}i\Omega_1{}^*\alpha_{32}{}^* - \tfrac{1}{2}i\Omega_2\alpha_{12} - i(\delta_1 - \delta_2)\alpha_{13}, \tag{1f}$$

In these equations, the usual rotating-wave, electric-dipole, and semiclassical field approximations are employed. The electric field is assumed to have the following form:

$$\mathbf{E}(\mathbf{r}, t) = \tfrac{1}{2}(\mathbf{E}_1(\mathbf{r})\exp(- i\omega_1 t) + \text{c.c.})$$
$$+ \tfrac{1}{2}(\mathbf{E}_2(\mathbf{r})\exp(- i\omega_2 t) + \text{c.c.}). \tag{2}$$

All remaining notations are defined in Table 1.

By making the three additional approximations listed in Table 2, the density-matrix equations can be reduced to the following simple form:

$$\frac{d}{dt}\begin{bmatrix} 2\,\text{Re}\,\alpha_{13} \\ 2\,\text{Im}\,\alpha_{13} \\ \rho_{11} - \rho_{33} \end{bmatrix} = A\begin{bmatrix} 2\,\text{Re}\,\alpha_{13} \\ 2\,\text{Im}\,\alpha_{13} \\ \rho_{11} - \rho_{33} \end{bmatrix} + B, \tag{3a}$$

where the observable fluorescence can be obtained from the following:

$$\rho_{22} = \frac{\Omega^2 Sf}{\gamma_2}\left[N + d(\rho_{11} - \rho_{33}) + g(2\,\text{Re}\,\alpha_{13})\right]. \tag{3b}$$

Here,

$$A = \begin{bmatrix} -[1 - g^2(1 - f)]\Omega^2 S & (\Delta - d\Omega^2 D) & gd(1 - f)\Omega^2 S \\ -(\Delta - d\Omega^2 D) & -\Omega^2 S & -g\Omega^2 D \\ [rdf + gd(1 - f)]\Omega^2 S & g\Omega^2 D & [rdf - 1 + d^2(1 - f)]\Omega^2 S \end{bmatrix}, \tag{3c}$$

$$B = N\Omega^2 S\begin{bmatrix} -gf \\ 0 \\ (r - d)f \end{bmatrix}. \tag{3d}$$

$N$ is the total number of atoms in the system, and the remaining quantities are defined in Table 3. These equations represent the complete solution of the Raman process in the interaction zones, within the listed approximations.

In the dark zone, the density-matrix equations simplify to

$$\frac{d}{dt}\begin{bmatrix} 2\,\text{Re}\,\alpha_{13} \\ 2\,\text{Im}\,\alpha_{13} \\ \rho_{11} - \rho_{33} \end{bmatrix} = \begin{bmatrix} 0 & \Delta & 0 \\ -\Delta & 0 & 0 \\ 0 & 0 & 0 \end{bmatrix}\begin{bmatrix} 2\,\text{Re}\,\alpha_{13} \\ 2\,\text{Im}\,\alpha_{13} \\ \rho_{11} - \rho_{33} \end{bmatrix} \tag{4a}$$

and

$$\rho_{22} = 0. \tag{4b}$$

Clearly, to compute the Ramsey-fringe line shapes one must combine these two solutions. To illustrate this, the approximations listed in Table 4 will be employed in order to simplify the problem. With these approximations, the den-

#### Table 1. Definitions Used in Eq. (1)

| Description | Defining Equation |
|---|---|
| Laser detuning of $\omega_1$ | $\delta_1 = \omega_1 - (\epsilon_2 - \epsilon_1)/\hbar$ |
| Laser detuning of $\omega_2$ | $\delta_2 = \omega_2 - (\epsilon_2 - \epsilon_3)/\hbar$ |
| Unperturbed energy levels | $\epsilon_1, \epsilon_2, \epsilon_3$ |
| Rabi frequency for 1–2 transition | $\Omega_1 = (\mu_{21} \cdot \mathbf{E}_1)/\hbar$ |
| Rabi frequency for 3–2 transition | $\Omega_2 = (\mu_{23} \cdot \mathbf{E}_2)/\hbar$ |
| Rotating-wave density-matrix elements | $\begin{cases} \alpha_{12} = \rho_{12}\exp(-i\omega_1 t) \\ \alpha_{32} = \rho_{32}\exp(-i\omega_2 t) \\ \alpha_{13} = \rho_{13}\exp(-i(\omega_1 - \omega_2)t) \end{cases}$ |
| Within-system decay rates | $\Gamma_{21}, \Gamma_{23}$ |
| Total state 2 decay rate | $\gamma_2$ |

#### Table 2. Approximations Used in Eq. (3)

| Description | Mathematical Form |
|---|---|
| State 2 short-lived compared with single-zone transit-time partial steady state | $\begin{cases} \dot{\rho}_{22} \ll \gamma_2\rho_{22} \\ \dot{\alpha}_{12} \ll (\tfrac{1}{2}\gamma_2 + i\delta_1)\alpha_{12} \\ \dot{\alpha}_{32} \ll (\tfrac{1}{2}\gamma_2 + i\delta_2)\alpha_{32} \end{cases}$ |
| Small laser difference frequency detuning (compared with correlated laser detuning or state 2 decay rate) | $\delta_1 - \delta_2 \ll \delta_1, \delta_2, \gamma_2$ |
| Closed system | $\Gamma_{21} + \Gamma_{23} = \gamma_2$ |

#### Table 3. Definitions Used in Eq. (3)

| Description | Defining Equation |
|---|---|
| Common-mode laser detuning | $\delta = \tfrac{1}{2}(\delta_1 + \delta_2)$ |
| Laser difference frequency detuning | $\Delta = (\delta_1 - \delta_2)$ |
| Average (squared) Rabi frequency | $\Omega^2 = \tfrac{1}{2}(|\Omega_1|^2 + |\Omega_2|^2)$ |
| Raman damping rate | $\Omega^2 S = \Omega^2 \dfrac{\gamma_2}{\gamma_2{}^2 + 4\delta^2}$ |
| Raman dispersion | $\Omega^2 D = \Omega^2 \dfrac{\delta}{\gamma_2{}^2 + 4\delta^2}$ |
| Normalized difference of (squared) Rabi frequencies | $d = \dfrac{|\Omega_1|^2 - |\Omega_2|^2}{|\Omega_1|^2 + |\Omega_2|^2}$ |
| Normalized product of Rabi frequencies | $g = 2\dfrac{|\Omega_1\Omega_2{}^*|}{|\Omega_1|^2 + |\Omega_2|^2}$ |
| Raman saturation parameter | $f = \dfrac{\gamma_2}{\gamma_2 + 3\Omega^2 S}$ |
| Normalized difference of within-system decay rates | $r = \dfrac{\Gamma_{21} - \Gamma_{23}}{\gamma_2}$ |

#### Table 4. Approximations Used in Eq. (5)

| Description | Defining Equation |
|---|---|
| Equal Rabi frequency | $d = 0, g = 1$ |
| Equal within-system decay rates | $r = 0$ |
| Small laser difference frequency detuning (compared with single-zone linewidth) | $\Delta \ll \Omega^2 S$ |

sity-matrix equations in the interaction zones reduce to the following:

$$\frac{d}{dt}\begin{bmatrix} 2\,\mathrm{Re}\,\alpha_{13} \\ 2\,\mathrm{Im}\,\alpha_{13} \\ \rho_{11} - \rho_{33} \end{bmatrix}$$

$$= \begin{bmatrix} f\Omega^2 S & 0 & 0 \\ 0 & -\Omega^2 S & -\Omega^2 D \\ 0 & \Omega^2 D & -\Omega^2 S \end{bmatrix}\begin{bmatrix} 2\,\mathrm{Re}\,\alpha_{13} \\ 2\,\mathrm{Im}\,\alpha_{13} \\ \rho_{11} - \rho_{33} \end{bmatrix} + N\begin{bmatrix} -f\Omega^2 S \\ 0 \\ 0 \end{bmatrix} \quad (5a)$$

and

$$\rho_{22} = \frac{\Omega^2 Sf}{\gamma_2}(N + 2\,\mathrm{Re}\,\alpha_{13}). \quad (5b)$$

The initial conditions for solving these equations are simple at zone A: $\alpha_0{}^{13} = 0$, and $(\rho_{11}{}^0 - \rho_{33}{}^0)$ is determined by optical pumping in the reference zone. For the dark zone and zone B, the initial conditions are of course obtained from the solution to the previous zone. Performing this calculation, for a rectangular laser beam profile, leads to the following expression[11] for the observable (spatially integrated) fluorescence in zone B:

$$\int_T^{T+T_B} \gamma_2 \rho_{22}\,dt = N[1 - \exp(-f\Omega^2 S_B\tau_B)]$$

$$\times \{1 + [1 - \exp(-f\Omega^2 S_A\tau_A)]|\sec\phi|\cos(\Delta T - \phi)\}, \quad (6a)$$

where $\phi$ is the phase of the complex Raman–Ramsey fringes and is given by

$$\tan\phi = \frac{\mathrm{Im}\,\alpha_{13}(\tau_A)}{\mathrm{Re}\,\alpha_{13}(\tau_A)}$$

$$= -\frac{(\rho_{11}{}^0 - \rho_{33}{}^0)\sin(\Omega^2 D_A\tau_A)\exp(-\Omega^2 S_A\tau_A)}{N[1 - \exp(-f\Omega^2 S_A\tau_A)]}. \quad (6b)$$

Here $\tau_A$ and $T_s$ are the transit times in zones A and B, respectively, and $T$ ($\gg\tau_A, \tau_B$) is the dark-zone transit time. Note that the phase shift depends totally on zone A (no zone B contribution) and in fact is equal to the phase of the (complex) Raman polarization, $\alpha_{13}(\tau_A)$, at the end of zone A. Other features of this expression will be illustrated below.

When unequal laser intensities are included, the expression for the Ramsey-fringe phase become

$$\tan\phi = -\frac{(\rho_{11}{}^0 - \rho_{33}{}^0)\sin(\Omega^2 D\tau)\exp(-\Omega^2 S\tau)}{N[1 - \exp(-f\Omega^2 S\tau)] + \xi d}, \quad (7a)$$

where

$$\xi = (\rho_{11}{}^0 - \rho_{33}{}^0)\{\cos(\Omega^2 D\tau) - \exp[(1 - f)\Omega^2 S\tau]\}\exp(-\Omega^2 S\tau) \quad (7b)$$

and the zone A subscripts have been dropped for simplicity. This expression shows that the ac Stark shift for unequal Rabi frequencies ($d \neq 0$, where $d$ is defined in Table 3) is nearly identical to the equal Rabi frequency case, except for an additional term, $d\xi$, in the denominator. Under the conditions of our experiment this additional term is small. Thus the two-zone ac Stark shift is not highly sensitive to

differences in laser intensities as long as the sum of the two Rabi frequencies (or laser intensities) remains unchanged.

## COMPARISON OF THEORY AND EXPERIMENT

Figure 6 shows six theoretical plots of the two-zone ac Stark shift [Eq. 6(b)] versus laser detuning. Each plot was generated by using values of laser intensities and initial atomic state populations obtained from the experimental conditions of the corresponding data in Fig. 5. No free parameters were used. As can be seen, these theoretical plots agree qualitatively with the experimental results, even though the theory assumes rectangular laser intensity profiles[10,11] and single-velocity atoms.[12,13] In particular, the calculations successfully predict the suppression of the two-zone ac Stark shift for increasing laser intensities (near zero detuning) as well as the general increase in ac Stark shifts with increasing initial population differences. The only discrepancy is the failure of the theory to predict correctly the reversal of slope seen in the lower left-hand experimental trace of Fig. 5. It will be shown below how this can be explained by using the fact that sodium is not a three-level system.

To test the predicted insensitivity of the ac Stark shift to differences in Rabi frequencies (or intensities) of the two laser fields, additional data were obtained for unequal Rabi frequencies. These data are shown in the top trace of Fig. 7 for the case when the laser field at $\omega_1$ has twice the intensity ($\sqrt{2}$ times the Rabi frequency) of the laser field at $\omega_2$ ($d = 1/3$, where $d$ is defined in Table 3). For these data the average intensity is $\Omega = 0.12\gamma_2$, and the initial atomic state population difference is $\rho_{11}{}^0 - \rho_{33}{}^0 = 0.8$. These values are similar to those of the bottom right-hand trace in Fig. 5. A theoretical plot corresponding to these data appears as the middle trace in Fig. 7. As in the equal-Rabi-frequency case, the agreement between theory and experiment is good. The
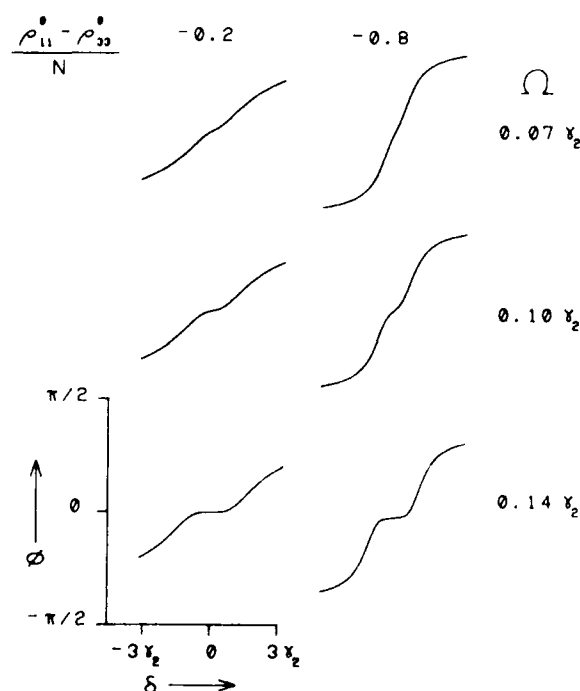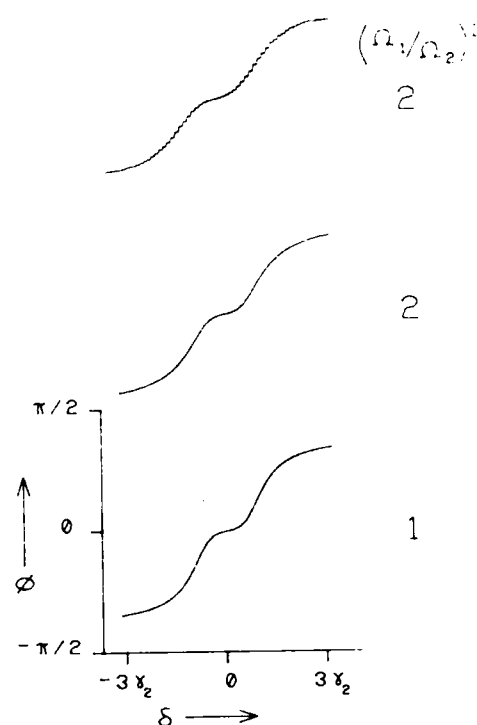


Fig. 7. Illustration of the insensitivity of the ac Stark shift to differences in Rabi frequencies. (Top trace) Data showing the ac Stark shift for unequal Rabi frequencies, $|\Omega_1/\Omega_2| = \sqrt{2}$. (Middle trace) Theoretical ac Stark shift for $|\Omega_1/\Omega_2| = \sqrt{2}$. (Bottom trace) Theoretical ac Stark shift for $|\Omega_1| = |\Omega_2|$ but same ($|\Omega_1|^2 + |\Omega_2|^2$).
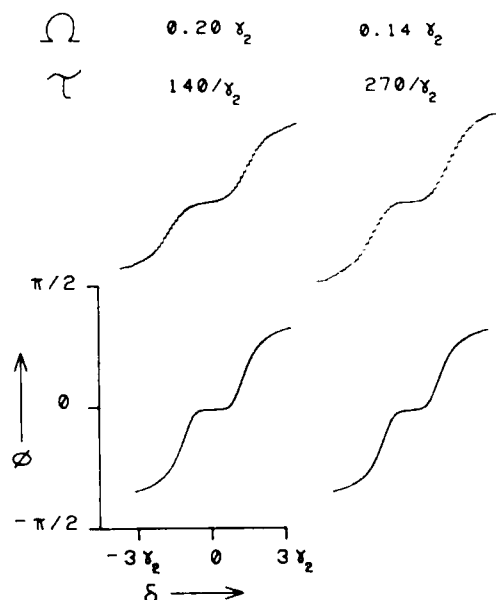


Fig. 8. Illustration of insensitivity of the ac Stark shift to the exact laser beam profile. Zone A transit times, $\tau$, are as indicated ($\Omega^2\tau$ remains constant). Top traces are experimental, bottom traces are theory.

bottom trace is included for comparison and was calculated by using the equal-Rabi-frequency expression [Eq. (6b)] for the same average Rabi frequency, $\Omega^2 = \frac{1}{2}(|\Omega_1|^2 + |\Omega_2|^2)$. Clearly, in this case the ac Stark shift is nearly insensitive to the differences in the Rabi frequencies for the 1-2 and 3-2 transitions.

To test the effects of different laser beam profiles on the two-zone ac Stark shift, Fig. 8 shows data obtained for two



Fig. 6. Calculated ac Stark shift, for conditions corresponding to the data presented in Fig. 5.

different laser beam sizes (in both zones A and B), where the intensities are adjusted such that the time-integrated intensity as seen by the moving atom ($\Omega^2\tau$ for rectangular profile) is the same. In a two-level system, this would be analogous to using, for example, two $\pi$ pulses ($\Omega\tau = \pi$) of different shape. The upper right-hand trace in Fig. 8 corresponds to a large laser beam and in fact is a reproduction of the lower right-hand trace in Fig. 5. Next, the laser power is reduced by approximately half, and the laser beams are focused to approximately half of the original diameters in both zones A and B. Data obtained under these conditions are shown in the upper left-hand trace of Fig. 8. As can be seen, the two upper traces of Fig. 8 are nearly identical, verifying that the exact laser beam profile is relatively unimportant, as long as the time-integrated intensity as seen by the moving atom remains unchanged.[11] The bottom two traces in Fig. 8 show the corresponding theoretical plots, obtained from Eq. (6b). Again, theory and experiment show qualitative agreement.

# THEORY INCLUDING ZEEMAN SUBLEVELS OF SODIUM

As mentioned above, agreement between experiment and theory was generally good except for the case (lower-left-hand trace of Fig. 5) in which a slope reversal near zero detuning was seen experimentally but not predicted theoretically. To explain this, it is necessary to consider the fact that sodium is not a perfect three-level system but has many Zeeman sublevels. Figure 9 shows the Zeeman sublevels of the sodium hyperfine states involved in the Raman interaction in our experiment. The allowed Raman transitions between these Zeeman levels (for right-circularly polarized laser light, as used in the experiment) are shown as solid lines. As mentioned above, a small ($\sim$60-mG) magnetic field, directed parallel to the laser **k** vectors, is used to lift the Zeeman degeneracy. The two heavy solid lines show the $m = 0$, $\Delta m = 0$ Raman transition that was used for our two-zone studies. The dotted lines show the additional transitions allowed for fluorescent decay. Relative matrix elements (squared) are shown near the bottom levels.

As can be seen from Fig. 9, state 2 decays to levels other than states 1 and 3, just as states 1 and 3 see an influx of atoms from upper Zeeman sublevels other than state 2. Because of these additional decay paths, the influx of populations to states 1 and 3 is not determined entirely by the within-system decay rates from state 2, as was the case for a closed three-level system. We are currently investigating the complex dynamics of the sodium system, using numerical methods. However, it should be possible to include the effects of the additional Zeeman levels to first order by introducing effective, unequal within-system decay rates, $\Gamma_{21} \neq \Gamma_{23}$ (or $r \neq 0$), to the closed three-level system equations. When this is done, the Ramsey-fringe phase is given by

$$\tan\phi = -\frac{(\rho_{11}{}^0 - \rho_{33}{}^0)[\sin(\Omega^2 D\tau)]\exp(-\Omega^2 S\tau) + r\zeta}{N\{1 - \exp[-(f - rdf)\Omega^2 S\tau]\} + d\xi' - r\eta}, \quad (8a)$$

where

$$\zeta = \tfrac{1}{2}f\Omega^2 S[EH - FG][N + d(\rho_{11}{}^0 - \rho_{33}{}^0)], \quad (8b)$$

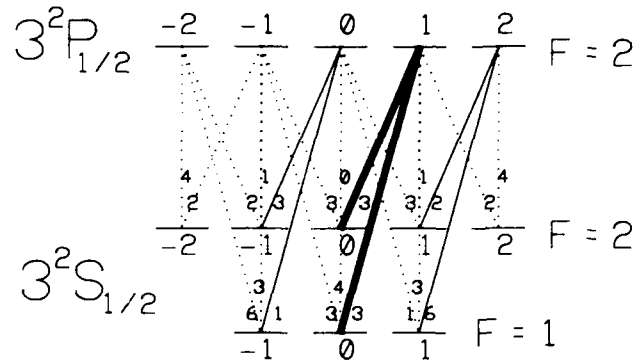$$\eta = \tfrac{1}{2}df\Omega^2 S[EG + FH][N - d(\rho_{11}{}^0 - \rho_{33}{}^0)], \quad (8c)$$



Fig. 9. Sodium hyperfine states involved in Raman interaction, for circularly polarized light. Solid lines are possible Raman transitions. Heavy solid lines show the $m = 0$, $\Delta m = 0$ Raman transitions used in these two-zone studies. Dotted lines are spontaneous decay paths. Number are relative matrix elements squared.
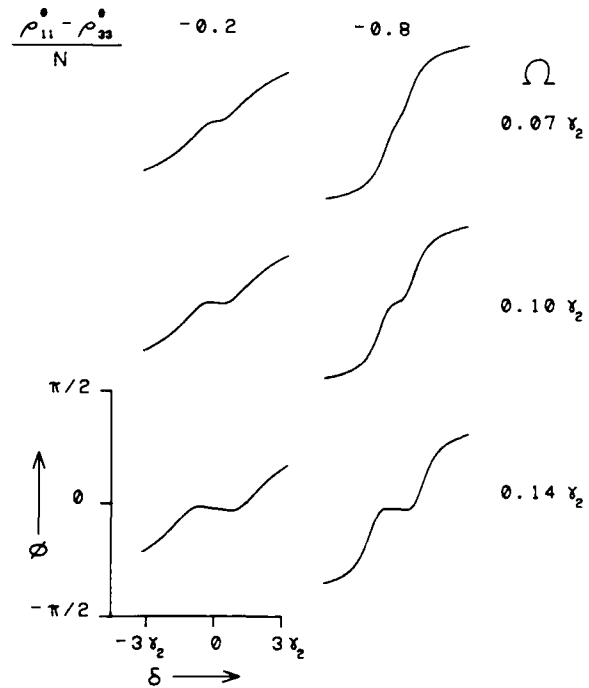


Fig. 10. Revised theoretical plots of the ac Stark shift, for conditions corresponding to the data presented in Fig. 5. Effects of nearby magnetic sublevels are included to first order by using an effective normalized difference of within-system decay rates, $r' = 0.275$.

$$\xi' = (\rho_{11}{}^0 - \rho_{33}{}^0)E, \quad (8d)$$

$$E = \{\cos(\Omega^2 D\tau) - \exp[(1 - f + rdf)\Omega^2 S\tau]\}\exp(-\Omega^2 S\tau), \quad (8e)$$

$$F = [\sin(\Omega^2 D\tau)]\exp(-\Omega^2 S\tau), \quad (8f)$$

$$G = \frac{2\Omega^2 S(1 - f + rdf)}{[\Omega^2 S(1 - f + rdf)]^2 + [\Omega^2 D]^2}, \quad (8g)$$

$$H = \frac{-2\Omega^2 D}{[\Omega^2 S(1 - f + rdf)]^2 + [\Omega^2 D]^2}, \quad (8h)$$

and, as before, the phase shift is determined entirely by the zone A interaction.

To estimate an effective value of $r$ (denoted by $r'$), it is first necessary to compute the total rate of population influx to states 1 and 3 from all levels. These rates will be called $\Gamma_{21}{}'$

and $\Gamma_{23}'$, respectively. The effective value of $r$ is then simply $r' = (\Gamma_{21}' - \Gamma_{23}')/(\Gamma_{21}' + \Gamma_{23}')$. To illustrate this, values of $r'$ will now be computed for two cases. First, assuming nearly equal initial populations in all the Zeeman ground-state sublevels, we compute an effective value of $r' = 0.22$, neglecting any optical pumping. Second, it is assumed that the $F = 1$ hyperfine ground sublevels are initially unpopulated but that the Zeeman sublevels in the $F = 2$ ground state are equally populated. Such an initial population distribution might be produced, for example, by a strong reference beam. In this case $r' = 0.33$. Averaging this and the previous value of $r'$ gives $r' = 0.275$.

Using this effective value of $r$ in Eqs. (8) results in the theoretical plots of Fig. 10, where as before the laser intensities and initial atomic state populations are obtained from the corresponding data in Fig. 5. As can be seen, the lower left-hand plot in Fig. 10 now shows much better agreement with the data. In particular, the slope reversal of the ac-Stark shift versus laser detuning is now correctly predicted.[14]

## SUPPRESSION OF ac STARK SHIFTS

Theoretically, inspection of Eqs. (6b) and (7a) predicts that the two-zone ac Stark shift should be exactly zero if the initial population difference between states 1 and 3 is zero. In the present sodium experiment this is not observed because optical pumping between Zeeman levels in the interaction zones always redistributes the populations somewhat. If a closed three-level system cannot be found, theory predicts that the ac Stark shift can still be reduced to arbitrarily small levels by strongly saturating the zone A interaction (i.e., high laser intensities or long interaction times).

In the present setup, however, we are limited in our choice of atomic systems and in our maximum laser intensities and interaction times. Nonetheless, the observed reversal of slope in the ac Stark shift near zero laser detuning suggests that for a range of (fixed) laser intensities, the initial atomic state populations can be adjusted so as to reduce the ac Stark shift greatly, even within the limitations of the present setup.

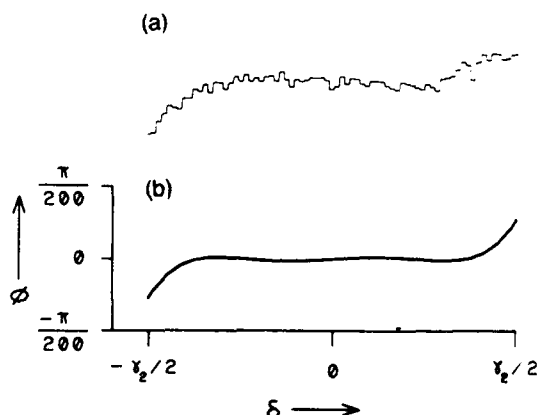To this end, Fig. 11(a) shows a high-resolution experimental plot of the ac Stark shift versus laser detuning obtained



Fig. 11. High-resolution ac Stark shift versus laser detuning: (a) experimental trace for $\Omega = 0.13\gamma_2, (\rho_{11}^0 - \rho_{33}^0) = 0.7N$, and (b) corresponding theoretical best fit, with $r' = 0.27$.

under the following experimental conditions, chosen so as to minimize the ac Stark shift near zero laser detuning: $\Omega = 0.13\gamma_2, (\rho_{11}^0 - \rho_{33}^0) = 0.7 N$. These data are shot-noise limited, obtained with an averaging time of 1 sec.

As can be seen from Fig. 11(a), the ac Stark shift is less than the noise over a laser detuning of nearly $\pm 0.2\gamma_2$. For comparison, Fig. 11(b) shows the theoretical ac Stark shift under these experimental conditions, where $r'$ is used as a free parameter to produce the flattest trace. Clearly, good agreement between theory and experiment is achieved, where the fitted value of $r'$ is 0.270, which is close to the approximated value of 0.275. Of course, a complete numerical treatment of the sodium system would not require the use of any free parameters. Nonetheless, Fig. 11 shows that even a simple first-order correction to the closed three-level system results is sufficient to give good agreement with data under the conditions of our experiment.

The data of Fig. 11(a) demonstrate an ac Stark shift of less than 0.0014 rad over a laser detuning of nearly $\pm 0.2\gamma_2$. For clock applications, this corresponds to a projected stability of better than $2 \times 10^{-11}$ for a laser detuning of $0.01\gamma_2$ (100 kHz for sodium). Here it should be noted that this result is still preliminary and does not represent the ultimate achievable clock performance. Nonetheless, these data demonstrate that, by proper choice of experimental conditions, the ac Stark shift can be greatly reduced, even within the limitations of the present experimental setup.

## SUMMARY AND FUTURE WORK

We have measured the ac Stark effect in a two-zone stimulated Raman interaction in a sodium atomic beam. In addition, we have derived simple theoretical expressions for the ac Stark shift, based on a closed three-level system, in the $\Lambda$ configuration and have achieved qualitative agreement with the data. In particular, the magnitude and sense of the ac Stark shifts are found to depend on laser intensities as well as on the initial populations of the two low-lying levels of the $\Lambda$ configuration. Specifically, the ac Stark shifts are smaller for larger laser intensities and also for smaller initial population differences between the two low-lying levels. Moreover, the ac Stark shift is shown to be insensitive to the ratio of the intensities of the two laser frequencies, provided that the sum of the two intensities is fixed. The ac Stark shift is also shown to be insensitive to changes in laser-beam profiles as long as the time-integrated intensity as seen by the moving atom remains unchanged. Quantitative agreement between ideal three-level theory and experiment is improved when the effects of the numerous Zeeman sublevels in sodium are taken into account to first order. Finally, the experimentally observed reversal of ac Stark shift was used in identifying conditions under which the ac Stark shift can be reduced to levels low enough to be acceptable for potential clock applications.

Future plans are to verify that the ac Stark shift can be further suppressed by increasing the degree of Raman saturation (i.e., large $\Omega^2 S\tau$). This can be achieved either by increasing the laser intensity or by slowing down the atoms (by cooling, for example). In addition, numerical calculations are in progress to identify the exact role played by the Zeeman sublevels and also to include the effects of velocity averaging.[12]

## REFERENCES AND NOTES

1. For example, B. J. Dalton, T. D. Kieu, and P. L. Knight, "Theory of ultra-high-resolution optical Raman Ramsey spectroscopy," Opt. Acta **33**, 459 (1986); D. Pegg, "Interaction of three-level atoms with modulated lasers," Opt. Acta **33**, 363 (1986); N. I. Shamrov, "Induced transparency in resonant induced Raman scattering," Zh. Prikl. Spektrosk. **40**, 346 (1984); S. Swain, "Conditions for population trapping in a three-level system," J. Phys. B **15**, 3405 (1982); P. M. Radmore and P. L. Knight, "Population trapping and dispersion in a three-level system," J. Phys. B **15**, 561 (1982); G. Orriols, "Nonabsorption resonances by nonlinear coherent effects in a three-level system," Nuovo Cimento B **53**, 1 (1979); H. R. Gray, R. M. Whitley, and C. R. Stroud, Jr., "Coherent trapping of atomic populations," Opt. Lett. **3**, 218 (1978); A. Szöke and E. Courtens, "Time-resolved resonance fluorescence and resonance Raman scattering," Phys. Rev. Lett. **34**, 1053 (1975).

2. P. L. Knight, M. A. Lauder, P. M. Radmore, and B. J. Dalton, "Making atoms transparent: trapped superpositions," Acta Phys. Austriasca **56**, 103 (1984); F. H. Mies and Y. B. Aryeh, "Kinetics and spectroscopy of near-resonant optical pumping in intense fields," J. Chem. Phys. **74**, 53 (1981); E. Courtens and S. Szöke, "Time and spectral resolution in resonance scattering and resonance fluorescence," Phys. Rev. A **15**, 1588 (1977); M. Sargent III and P. Horwitz, "Three-level Rabi flopping," Phys. Rev. A **13**, 1962 (1976); R. G. Brewer and E. L. Hahn, "Coherent two-photon processes: transient and steady state cases," Phys. Rev. A **11**, 1641 (1975).

3. J. Mlynek and R. Grimm, "Raman heterodyne Ramsey spectroscopy in a samarium atomic beam" Appl. Phys. B **45**, 77 (1988); M. Kaivola, P. Thorsen, and O. Poulsen, "Dispersive line shapes and optical pumping in a three-level system," Phys. Rev. A **32**, 207 (1985); F. Shimizu, K. Shimizu, and H. Takuma, "Selective vibrational pumping of a molecular beam by a stimulated Raman process," Phys. Rev. A **31**, 3132 (1985); A. Sharma, W. Happar, and Y. Q. Lu, "Sub-Doppler-broadened magnetic field resonances in the resonant stimulated electronic Raman scattering of multimode laser light," Phys. Rev. A **29**, 749 (1984); R. E. Tench and S. Ezekiel, "Precision measurements of hyperfine predissociation in I₂ vapor using a two-photon resonant scattering technique," Chem. Phys. Lett. **96**, 253 (1983); R. E. Tench, B. W. Peuse, P. R. Hemmer, J. E. Thomas, S. Ezekiel, C. C. Leiby Jr., R. H. Picard, C. R. Willis, "Two laser Raman difference frequency technique applied to high precision spectroscopy," J. Phys. Colloq. **42**, 45 (1981); P. Kumar and J. H. Shapiro, "Observation of Raman-shifted oscillation near the sodium *D* lines," Opt. Lett. **10**, 226 (1985); M. S. Feld, M. M. Burns, T. U. Kuhl, P. G. Pappas, and D. E. Murnick, "Laser-saturation spectroscopy with optical pumping," Opt. Lett. **5**, 79 (1980); G. Alzetta, L. Moi, and G. Orriols, "Nonabsorption hyperfine resonances in a sodium vapor irradiated by a multimode dye-laser," Nuovo Cimento B **52**, 209 (1979); R. P. Hackel and S. Ezekiel, "Observation of unnatural linewidths by two-step resonant scattering in I₂ vapor," Phys. Rev. Lett. **42**, 1736 (1979); K. Takagi, R. F. Curl, and R. T. M. Su, "Spectroscopy with modulation sidebands," Appl. Phys. **7**, 181 (1975); R. L. Shoemaker and R. G. Brewer, "Two-photon superradiance," Phys. Rev. Lett. **28**, 1430, (1972).

4. E. Buhr and J. Mlynek, "Collision-induced Ramsey resonances in Sm vapor," Phys. Rev. Lett. **57**, 1300 (1986); A. A. Dabagyan, M. E. Movsesyan, T. O. Ovakimyan, and S. V. Shmavonyan, "Stimulated processes in potassium vapor in the presence of a buffer gas," Sov. Phys. JETP **58**, 700 (1983).

5. D. Krokel, K. Ludewigt, and H. Welling, "Frequency up-conversion by stimulated hyper-Raman scattering," IEEE J. Quantum Electron. **QE-22**, 489 (1986); R. S. F. Chang, M. T. Duignan, R. H. Lehmberg, and N. Djeu, "Use of stimulated Raman scattering for reducing the divergence of severely aberrated laser beams," in *Excimer Lasers: Their Applications and New Frontiers in Lasers*, R. W. Waynank, ed., Proc. Soc. Photo-Opt. Eng. **476**, 81 (1984); J. C. White, "Up-conversion of excimer lasers via stimulated anti-Stokes Raman scattering," IEEE J. Quantum Electron. **QE-20**, 185 (1984); N. V. Znamenskii and V. I. Odintsov, "Infrared stimulated Raman scattering in rubidium vapor with a tunable pump frequency," Opt. Spectrosc. (USSR) **54**, 55 (1983); R. Wyatt, N. P. Ernsting, W. G. Wrobel, "Tunable electronic Raman laser at 16 microns," Appl. Phys. B **27**, 175 (1982); M. L. Steyn-Ross and D. F. Walls, "Quantum theory of a Raman laser," Opt. Acta **28**, 201 (1981).

6. P. R. Hemmer, G. P. Ontai, and S. Ezekiel, "Precision studies of stimulated resonance Raman interactions in an atomic beam," J. Opt. Soc. Am. B **3**, 219 (1986); P. R. Hemmer, S. Ezekiel, and C. C. Leiby, Jr., "Stabilization of a microwave oscillator using a resonance Raman transition in a sodium beam," Opt. Lett. **8**, 440 (1983); P. Knight, "New frequency standards from ultra-narrow Raman resonances," Nature (London) **297**, 16 (1982); J. E. Thomas, P. R. Hemmer, S. Ezekiel, C. C. Leiby, Jr., R. H. Picard, and C. R. Willis, "Observation of Ramsey fringes using a stimulated resonance Raman transition in a sodium atomic beam," Phys. Rev. Lett. **48**, 867 (1982); J. E. Thomas, S. Ezekiel, C. C. Leiby, Jr., R. H. Picard, and C. R. Willis, "Ultrahigh resolution spectroscopy and frequency standards in the microwave and far-infrared region using optical lasers," Opt. Lett. **6**, 298 (1981).

7. P. R. Hemmer, V. D. Natoli, M. S. Shahriar, B. Bernacki, H. Lamela-Rivera, S. P. Smith, and S. Ezekiel, in *41st Annual Symposium on Frequency Control* (Institute of Electrical and Electronics Engineers, New York, 1987), p. 42.

8. E. De Clercq and P. Cerez, "Evaluation of the light shift in a frequency standard based on Raman induced Ramsey resonance," Opt. Comm. **45**, 91 (1983); B. J. Dalton and P. L. Knight, "The effects of laser field fluctuations on coherent population trapping," J. Phys. B. **15**, 3997 (1982).

9. N. F. Ramsey, *Molecular Beams* (Oxford U. Press, London, 1963), Chap. 5, Sec. 3.

10. Average laser intensity is defined here by the following:

$$\langle \Omega^2 \rangle_{\text{average}} = \frac{1}{\tau_{1/2}} \int_{-\infty}^{\infty} \Omega^2(t)\mathrm{d}t,$$

where $\tau_{1/2}$ is the atom transit time corresponding to the half-intensity positions on the actual laser beam profile and $\Omega^2 = \frac{1}{2}(|\Omega_1|^2 + |\Omega_2|^2$. Here, $|\Omega_1|^2$ and $|\Omega_2|^2$ are the laser intensities at $\omega_1$ and $\omega_2$, respectively, in units of Rabi frequency squared.

11. For a nonrectangular laser beam profile, $\Omega$ is a function of time for a moving atom in the atomic beam. In that case, Eqs. (6a) and (6b) are modified by making the making the following replacements:

$$\Omega^2\tau \rightarrow \int_{-\infty}^{\infty} \Omega^2(t)\mathrm{d}t, \qquad f\Omega^2\tau \rightarrow \int_{-\infty}^{\infty} f(t)\Omega^2(t)\mathrm{d}t$$

where it is assumed that the two interaction regions do not overlap, so that

$$\int (\Omega_A^2 + \Omega_B^2)\mathrm{d}t = \int \Omega_A^2\mathrm{d}t + \int \Omega_B^2\mathrm{d}t.$$

For the intensities used in our experiments, $f$ is nearly a constant (unity) and can be pulled outside the integral.

12. Interaction times and transit times are computed by using the thermal velocity $v = \sqrt{2kT/M}$ characteristic of a sodium beam produced by a 400°C oven.

13. In general, velocity averaging is accomplished by simply performing a weighted average over all the velocities present in the atomic beam. However, in the present case the ac Stark shift was measured by locking to a minimum of a velocity averaged

Ramsey-fringe line shape. This ac Stark shift is not the same as the weighted average of the ac Stark shifts for each atomic velocity. Nevertheless, over the limited ranges of common-mode laser detuning where $\phi$ and $\Delta T$ are both small (so that $\phi \simeq \sin \phi$ and $\Delta T \simeq \sin \Delta T$) for all velocities included in the average, a relatively simple numerical calculation is possible and is found to agree well with the single-velocity results presented here. Therefore it is anticipated that the complete numerical calcula-

tion of the Raman two-zone ac Stark effect, including velocity averaging in a thermal sodium beam, will probably give results that are qualitatively similar to those presented in this paper.

14. It should be pointed out that the effective value of $r$ as indicated is merely an estimate of the first-order correction to the closed three-level-system results. The exact solution of the sodium system is more complex than simply using an effective value of $r$ and is currently in progress.

# MISSION

## OF

## ROME LABORATORY

Rome Laboratory plans and executes an interdisciplinary program in research, development, test, and technology transition in support of Air Force Command, Control, Communications and Intelligence ($C^3I$) activities for all Air Force platforms. It also executes selected acquisition programs in several areas of expertise. Technical and engineering support within areas of competence is provided to ESD Program Offices (POs) and other ESD elements to perform effective acquisition of $C^3I$ systems. In addition, Rome Laboratory's technology supports other AFSC Product Divisions, the Air Force user community, and other DOD and non-DOD agencies. Rome Laboratory maintains technical competence and research programs in areas including, but not limited to, communications, command and control, battle management, intelligence information processing, computational sciences and software producibility, wide area surveillance/sensors, signal processing, solid state sciences, photonics, electromagnetic technology, superconductivity, and electronic reliability/maintainability and testability.